Direct Solution Synthesis of Transition Metal Borides

Md Mashroor Elahi Raiyan

A thesis
submitted in partial fulfillment of the
requirements for the degree of

Master of Science in Applied Chemical Science and Technology

University of Washington

2023

Committee:
Brandi M. Cossairt
Lilo D. Pozzo

Program Authorized to Offer Degree:
Chemistry

University of Washington

Abstract

Direct Solution Synthesis of Transition Metal Borides

Md Mashroor Elahi Raiyan

Chair of the Supervisor Committee:

Brandi M. Cossairt

Department of Chemistry

Recent years have seen an increase in the study of metal borides due to their multifaceted applications, ranging from abrasive materials to superconductors. This variety in function emerges from the distinctive bonding properties of boron, which gives rise to diverse structures and stoichiometries in metal borides. An area of significant exploration is the use of metal borides in the electrocatalysis of water, specifically in hydrogen evolution and oxygen evolution reactions, as well as hydrogen storage. Notably, successful hydrogen storage has only been achieved with MgB_2 (i.e., interconversion with $Mg(BH_4)_2$) among all the metal borides studied so far.

Synthesizing metal borides, however, presents a challenge. In response to this, I have investigated the direct solution synthesis using chemical reduction using a Schlenk techniques at 280 °C and using high pressure high temperature reactors at 180 °C. The materials studied included nickel boride, zirconium boride, cobalt boride, and a nickel-zirconium bimetallic boride. Although only the synthesis of nickel and zirconium borides were found to successfully produce well-defined crystalline nanoparticles, these outcomes provide promising indicators for future efforts in creating crystalline transition metal boride nanoparticles.

Acknowledgements

I would like to thank University of Washington Chemistry department for providing instruments and funding to help me with my research. I would also like to thank Dr. Brandi Cossairt, Dr. Ding-Yuan Kuo and Ricardo Rivera-Maldonado for being my mentors and guiding me through this research. The research was done in collaboration with research groups of Dr. Godwin Severa from University of Hawaii in Manoa and Dr. Lilo Pozzo at University of Washington Chemical Engineering department who have also helped me in finalizing the research project. A last thank you Molecular Analysis Facility scientists Dr. Samantha Young, Mrs. Ellen Lavoie and Mr. Scott Braswell who helped me with data collection for my samples with x-ray diffraction, scanning electron microscopy and transmission electron microscopy.

Part of this work was conducted at the Molecular Analysis Facility, a National Nanotechnology Coordinated Infrastructure (NNCI) site at the University of Washington, which is supported in part by funds from the National Science Foundation (awards NNCI-2025489, NNCI-1542101), the Molecular Engineering & Sciences Institute, and the Clean Energy Institute.

Table of contents

Table of figures

Table of figures **Page number**

Table of supplemental figures

Table of schemes

Table of tables

Introduction

Boron minerals form as borax mostly, from hot gases or springs near volcanic active sites.[1] Some examples of the main minerals are borax, hydrated sodium borate, kernite, colemanite, and hydrated calcium borate.[1] There are approximately 380 million tons of boric oxide as the main reserve of boron minerals around the world, and a large portion of the world's boron reserves are located in Turkey, Argentina, and China.[1]

Boron can adopt a variety of covalent hybridization modes (sp1, sp2 and sp3), and forms unusual molecular structures with multicenter B-B bonds due to its electron deficiency, i.e. having one less valence electron than its number of valence orbitals.[2,3] Boron reacts with most metals forming metal borides, which vary structurally and compositionally allowing them to be divided into three groups. The first group is the boron-rich metal borides, which have a small metal to boron ratio (M/B < 0.5, M = metal and B = boride), an example being YB_{66}.[2,4,5] The second group is the metal rich metal borides, which have a large metal to boron ratio (M/B > 2), an example being $Nd_2Fe_{14}B$.[2,5] The third group of metal borides are characterized by a moderate metal to boron ratio ($0.5 \leq M/B \leq 2$).[2,5]

Over the years the crystal structures of various types of metal borides have been studied theoretically and experimentally determined.[1–3,5–10] Metal borides demonstrate diverse functionality that is brought about compositional diversity across the periodic table, with a trend in B sublattice evolving from isolated clusters into one, two, or three-dimensional frameworks as the boron to metal ratio increases.[11]

i. STRUCTURES OF METAL RICH METAL BORIDES

In most metal rich borides, the boron atoms are placed in trigonal prisms formed by the metal atom layers, however other modes of boron coordination have also been reported, such as square antiprismatic (e.g. $CuAl_2$- type borides) and octahedral (e.g. boride perovskites).[2,10] $CeCo_3B_2$ is a good example of a metal rich boride that has trigonal prism coordination with isolated boron atoms surrounded by nine metal atoms forming said trigonal prism.[10] Each cobalt atom is surrounded by 12 atoms forming a tetragonal prism and each cerium atom is coordinated by 20 atoms forming a hexagonal prism.[10] The structure is shown below in figure 1:

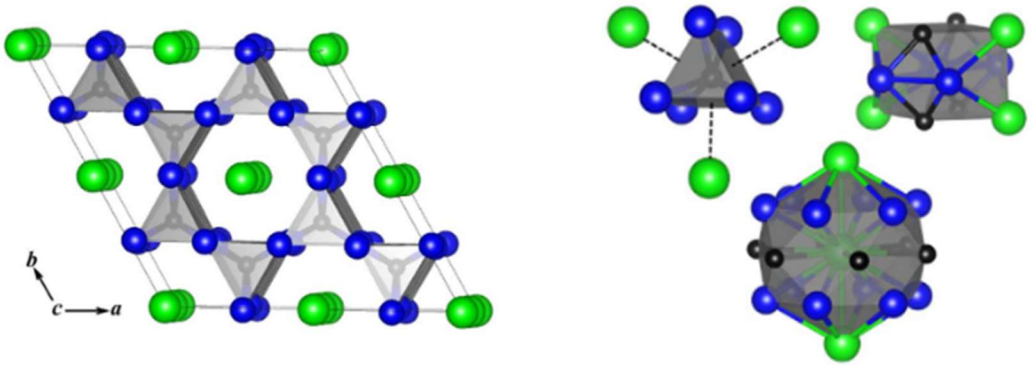

Figure 1. (left) Structure of $CeCo_3B_2$ as an example of metal rich boride with trigonal prism coordination. (right) Specific coordination of boron, cobalt and cerium in $CeCo_3B_2$. Cerrium atoms are shown in green, cobalt atoms shown in blue and boron atoms shown in black.[10]

ii. STRUCTURES OF BORON RICH METAL BORIDES

As mentioned earlier, the boron lattices evolve with the increase in boron to metal ratio. In the case of boron rich metal borides, such as yttrium borides, boron atoms form a layered hexagonal structure in YB_2, the boron atoms become interconnected in YB_4, and in YB_6 there are B_6 octahedra in the cubic structure.[11] In cases of higher order YB, boron atoms form cuboctahedra e.g. in YB_{12}, while YB_{25} and YB_{50} have B_{12} icosahedron.[11] As the boron content increases, the length of B-B bonds also decreases, which is all observed in figure 2 below:[11]

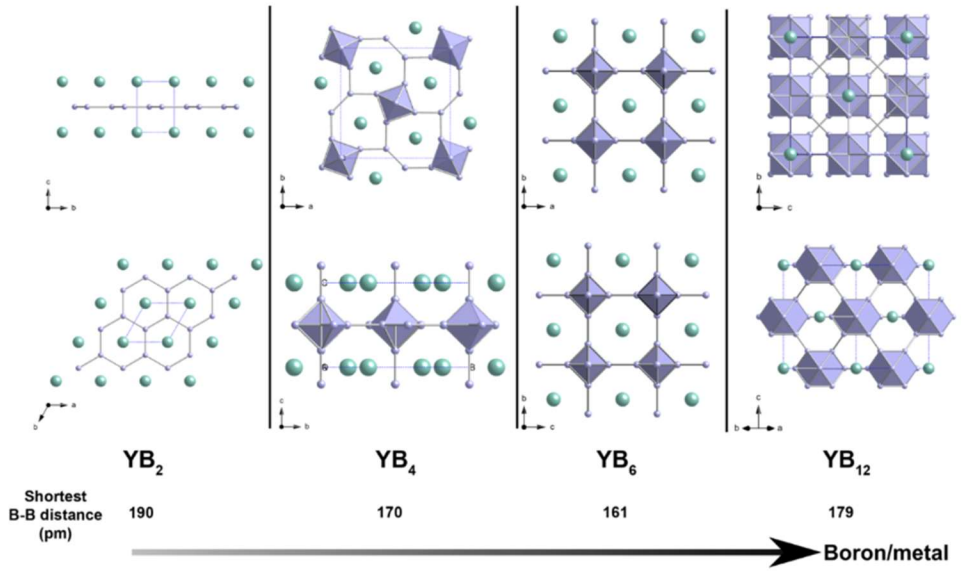

Figure 2. Crystal structure of YB_x as an example of boron rich borides. YB_2 is the simplest variant with simple hexagonal layered boron atom network with 190 pm B-B length. YB_{12} forms 3D network of boron cuboctahedra with small B-B length of 179 pm. Small grey spheres are boron atoms and large green spheres are yttrium atoms.[11]

YB_{66} is the most complex variant of yttrium boride where the B_{12} icosahedron connected together in a 3D network shown in figure 3:[11]

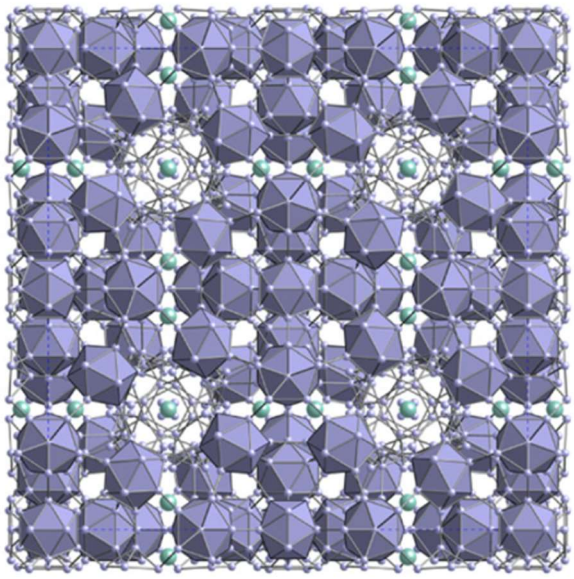

Figure 3. Single unit cell of YB_{66}. Small grey spheres are boron atoms forming polyhedra. Large green spheres are yttrium atoms.[11]

Dodecaborides of transition metals also fall under this category. They're usually of two structure types – UB_{12} and ScB_{12}.[3,12] The structures of dodecaborides in general constitute of boron cuboctahedron cages of 24 atoms, each containing a 12-coordinated metal in the center.[12] While in the UB_{12} type structures, the cages are arranged in a face-centered cubic closed packed system in ScB_{12}, the cuboctahedra are arranged in a body-centered tetragonal closed packed structure.[3,12] Structures of UB_{12} and ScB_{12} is shown in figure 4:

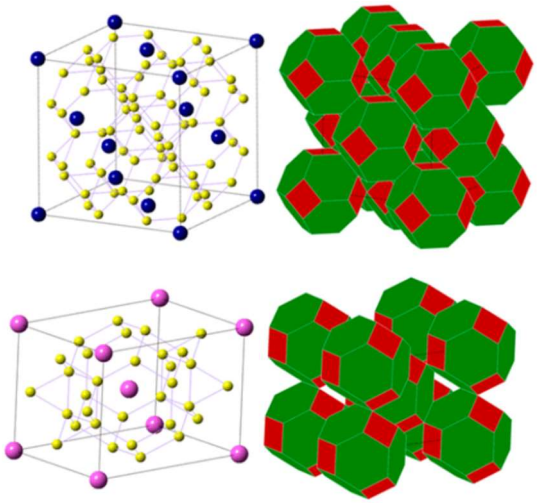

Figure 4. (Top left) unit cell of UB_{12}, metal atoms are in blue and boron atoms are in yellow. (Top right) face centered close packed coordinated cages of cuboctahedron. (Bottom left) ScB_{12} type structure unit cell. (Bottom right) body centered tetragonal packed cuboctahedra.[12]

iii. STRUCTURES OF TRANSITION METAL BORIDES

Most transition metal borides result in having moderate metal to boron ratio as compounds.[3] Transition metals have high electron density which combined with boron's unique electron deficiency property forms transition metal borides (TMBs) with ionic, metallic and covalent bonds.[2–4] Transition metal borides are grouped into four main classes – monoborides (TMB), diborides (TMB_2), tetraborides (TMB_4) and dodecaborides (TMB_{12}).[3]

Some examples of monoborides are CrB, VB, NiB, β-FeB, α-MoB etc[3]. They share some structural similarities between themselves; e.g. in both CrB and β-FeB, the boron are arranged in a zig-zag chain parallel to the α axis however, in β-FeB the inclination of the zig-zag chain is at a different angle.[3] The structure of α-MoB is different from the previous two in that the boron chain is perpendicular to the α axis.[3] These differences are better illustrated in figure 5 below:

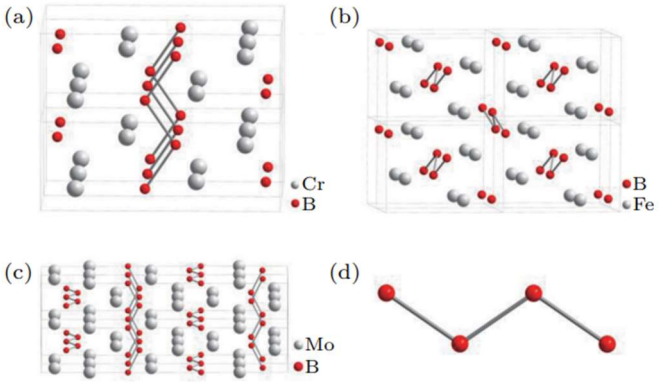

Figure 5. Structure of monoborides where B atoms are highlighted in red and metal atoms are highlighted in grey. A) CrB crystal structure with the zig zag boron chain parallel to the α axis. B) β-FeB crystal structure with similar zig zag chain parallel to α axis, but has different inclination compared to CrB. C) α-MoB crystal structure with perpendicular zig zag boron chain. D) boron atom chain in each crystal structure.[3]

It is important to note that although there are many different types of monoborides, their crystal structures are similar to the examples mentioned above. VB, α-FeB, NiB, etc. are some that share the same crystal structure with CrB; TiB, MnB, CoB share crystal structure with β-FeB and α-WB is the only other monoboride known to share the same crystal structure with α-MoB.[3]

Transition metal diborides are classified into five structural types – ReB_2, AlB_2, β-MoB_2, α-WB_2, and RuB_2 type.[3] The various TMB_2's present have structures that are the same as those previously mentioned. In the AlB_2 type structures, boron atoms form a graphite like boron layer in a honeycomb fashion, and transition metal atoms form closely packed layers aligned with the center of the honeycomb hexagon of boron atoms.[2,3] Some examples of diborides with the AlB_2 type structure are CrB_2, MnB_2, YB_2, ZrB_2 etc. The structure of AlB_2 type diborides is shown in figure 6:

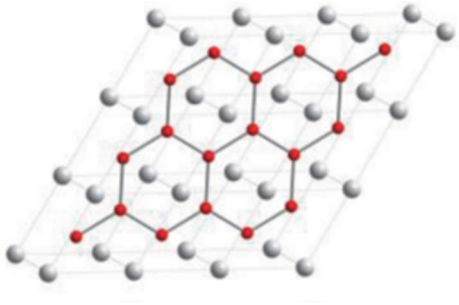

Figure 6. AlB_2 type diboride structure. Metal atoms are in grey and boron atoms are red. Overall structure is a trigonal prism with each boron atom neighboring six transition metal atoms near it.[3]

In β-MoB_2 the boron and transition metal layers alternate in a fashion similar to AlB_2 however, instead of just a 2D layer the structures have an alternating graphene boron layer and a quasi-3D wrinkled boron layer, shown in figure 7 down below:[3]

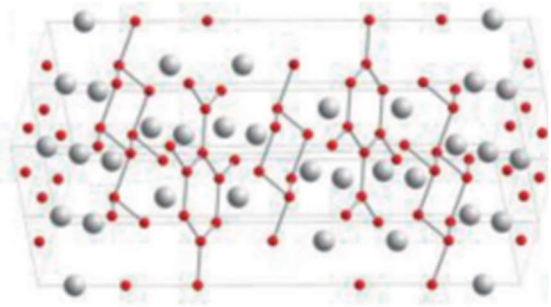

Figure 7. Crystal structure of β-MoB_2 type diborides. Metal atoms are shown in grey and boron atoms are shown in red. The boron layers are alternating between the graphene layer and quasi 3D wrinkled layer.[3]

In ReB_2 type structures the boron atoms form a condensed chair-like conformation with six rings that alternates with the metal atom layer.[3,8] The rhenium layer is in a hexagonal close packing with each atom coordinating with six other rhenium atoms in the same layer, shown in figure 8:[8]

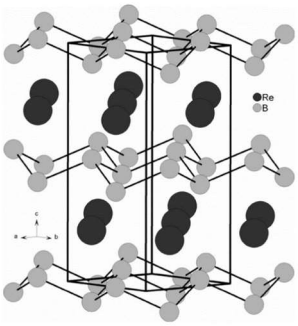

Figure 8. Crystal structure of ReB_2. Re atoms shown in black and B atoms shown in grey. Boron atoms form a chair configuration layer alternating with the metal layer in a hexagonal formation.[8]

In the structures of RuB_2 type diborides, the boron atom layer is in a conjugated boat configuration and undulates with the metal layer. The metal atoms are arranged in a hexagonal sheet and each metal atom neighbors with 6 other atoms in each respective layer.[8] OsB_2 is another diboride that shares the same structure with RuB_2.[3,8] The structure is shown in figure 9 below:

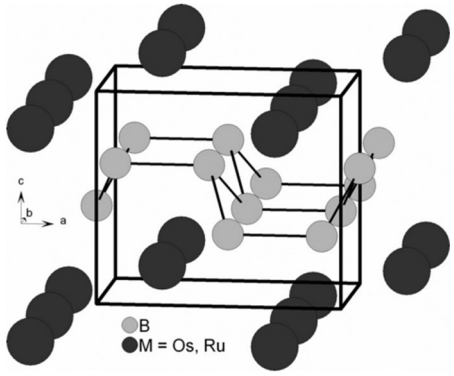

Figure 9. Crystal structure of RuB_2 type diborides. Metal atoms are shown in black and boron atoms are shown in grey. Boron atom layers are in a boat configuration alternating with the metal atom layer.[8]

There have not been any conclusive structures for the remaining type of general diboride structures - MnB_2, WB_2, and MoB_2. MnB_2 has exhibited both AlB_2 and ReB_2 type structures, with the latter being more stable from theoretical calculations.[3] While an AlB_2 type structure for WB_2 was theoretically determined, it has only been observed experimentally above 65 GPA.[3] MoB_2 has been theoretically calculated to have two

phases – α-MoB_2 and β-MoB_2; α-MoB_2 having a hexagonal crystal structural arrangement and β-MoB_2 being a rhombohedral crystal.

Regarding tetraborides not many TMB_4's have been synthesized but there is interest since these materials are characterized as superhard materials.[3] CrB_4 has an 3D orthorhombic crystal structure and can have two different space groups – *Immm* and *Pnmm*.[3,9] The difference between its *Immm* and *Pnmm* space group was the placement of the boron atom, which is titled in the *Pnmm* group. The differences can only be observed via neutron diffraction illustrated in figure 10 below:

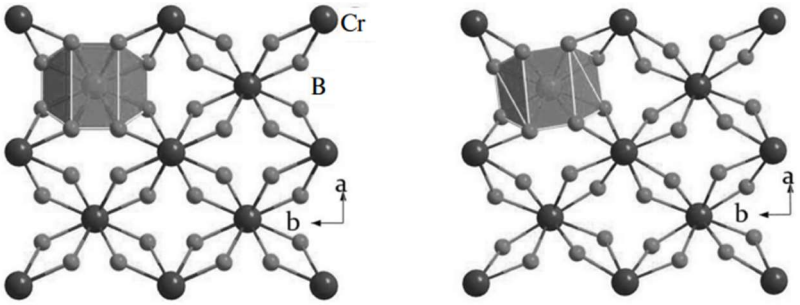

Figure 10. Neutron diffraction pattern showing crystal structure of CrB_4 in both space groups with *Immm* on the left and *Pnmm* on the right. Cr atoms shown in larger black circles and boron atoms are the smaller grey circles.[9]

Neutron diffraction shows the difference between the space groups is the position of the top left unit cell. When looking at the difference in space groups of CrB_4, neutron diffraction was necessary as XRD did not provide any difference between the two space group types seen in figure 11:

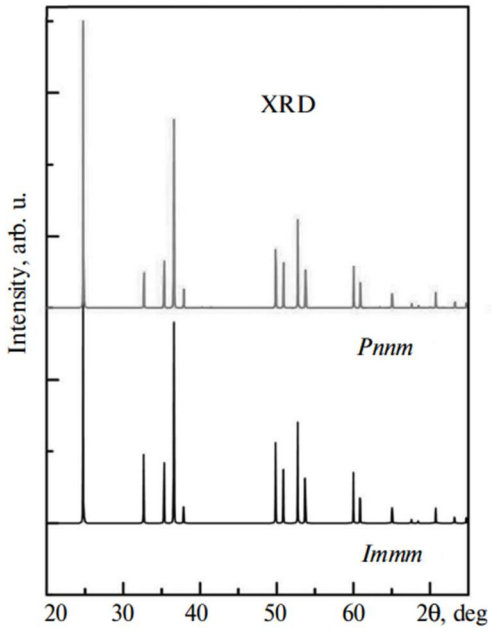

Figure 11. XRD of *Pnmm* (top) and *Immm* (bottom)space group of CrB_4.[9]

iv. APPLICATIONS OF METAL BORIDES

As mentioned before, metal borides have diverse functions and applications.[3,5–7,9–20] For example, due to their unique structures, TMBs such as ReB_2, OsB_2, and WB_4, etc. come close to being superhard materials.[3] Superhard materials are defined by materials that have Vickers hardness above 40 GPa at a particular applied load.[21] In cases of the aforementioned TMBs they have wrinkled or zig zag boron layers in a quasi 3D structure which allows for them to have their superhard property.[3] For others such as CrB and MnB, the monoborides have symmetrical electronic partition of the 3D metal-boride and zigzag boron-boron bonding network, resulting in higher Vickers hardness than the diboride or tetraborides (CrB_2, MnB_4).[3] However, they only have managed to get a Vickers number of 30 GPa due to the quantum mechanical effect involving the two center and three center boron atoms that reduce the rigidity of the materials.[3] Some notable examples of current superhard materials are diamond and cubic boron nitride (cBN).[3] The transition metal borides (ReB_2 OsB_2 and WB_4) have got close to superhard levels of 37 GPa approximately – making them possible future substitutes for cBN and diamond but more research is needed to determine structural or

chemical composition to achieve the 40 GPa mark.[3] If successful, this can let them be used as abrasive materials to grind ferrous metals and superalloys in aerospace and automotive engineering fields such as parts for camshafts, gears, transmission parts, turbine blades, nozzles etc.[13] They can also be used in optical instruments for submarines similar to CVD diamonds that are currently being used.[13]

Metal borides have also been researched for use in the field of superconductivity. Superconductivity in transition metals is difficult to achieve because of the d electron pairing not being favored by Bardeen-Cooper-Scheiffer (BCS) theory.[15] However, metal borides such as MgB_2, ZrB_{12}, ScB_{12}, etc. were observed to have superconductivity at low critical temperature (T_c) ranging from 5.5-8 K.[3] Besides superconductors, divalent hexaborides such as CaB_6, SrB_6, BaB_6 display semiconductor behavior because of nonstoichiometry and impurities from synthesis, while LaB_6 and EuB_6 are conductors because of the additional electron not monopolized by boron network.[14]

Metal borides such as 2D Mo_2B_2 and Fe_2B_2 have been found to have omnidirectional small diffusion barriers and high storage capacity for Li atoms making them candidates for electrodes in Li batteries. ZrB_2, AlB_2 and MgB_2 have also been used as refractory and energetic materials due to their high melting point and oxidation state in aerospace applications as fuels and propellants.[16,17] However, a growing field where metal boride applications are being explored is in hydrogen production and storage using transition metal borides.

Extracting energy from abundant small molecules like water (H_2O) has been emerging as an attractive solution to our global energy and climate challenges. Some of the best results have come from electrochemical water splitting using noble earth metals such as Ir, Pt, Ru etc.[19,20] While being highly efficient for the hydrogen evolution reaction (HER) and the oxygen evolution reaction (OER), these metals are very expensive and limited in supply on Earth.[19,20] In looking for alternatives to these, TMBs have gained interest in the past, but challenges include synthesizing TMBs at a bulk scale and finding the appropriate conditions for electrochemical water splitting procedures.[19,20] Table I has a summary of electrochemical water splitting with some example TMBs:

Table I. Different TMB electrocatalysts with their electrocatalytic function with appropriate conditions and Tafel slope

Electrocatalyst	Reaction	Medium	Tafel slope/ mV dec^{-1}
Ultrathin Ni_xB nanosheet	HER	1M KOH	89
Amorphous Co-B nanoparticles	HER	neutral	75
FeB_2 nanoparticles	OER	1M KOH	52.4
Amorphous Co_x-Fe-B	OER	1M KOH	62.6

There are a few problems with TMB application in electrochemical water splitting. First one being their long-term stability, which declines due to the exfoliation of the catalysts by bubble production and also by overoxidation of the electrocatalysts when using binders such as Nafion to tether nanostructured catalysts to a substrate.[20] Another problem TMBs face is inevitable surface oxidation when stored under air – with the oxidation forming oxides on the boron surface, forming borates or on the metal surface forming metal oxides.[20] The last big problem is developing function of TMB catalysts under acidic media. As seen from Table I, the TMB electrocatalysts only function under alkaline conditions, which otherwise cannot be done without noble metal catalysts.[20]

Besides water splitting and hydrogen production, metal borides are also emerging for application in hydrogen storage. To date, efficient storage has only been demonstrated in MgB_2 in nanosheet and bulk form.[18] The MgB_2 nanosheets after hydrogenation to $Mg(BH_4)_2$ at 70 MPa in 330 ºC followed by

dehydrogenation at 390 ºC achieved a hydrogen capacity of 5.1 wt% which is 50 times higher compared to bulk MgB_2 under the same conditions.[18] Unfortunately, hydrogen storage has not been achieved yet in TMBs and in general further research is needed to synthesize TMBs for real world applications in these matters.

v. SYNTHESIS OF METAL BORIDES

One central challenge in the study and application of TMBs is synthesizing them; whether it is films, nanocrystals, or different 3D and 2D structures that affect their mechanical and electrical properties.[2,3,5,9,10,19,20] At present TMBs, especially boron rich phases (e.g. ZrB_{12}, YB_{66}) that have strong covalent bonds, require high temperature and high pressure conditions (HPHT) to synthesize efficiently.[3] With high pressure conditions being introduced, the distance between atoms are further reduced and overlap of electron clouds allows for stronger bond formation, and thus allowing for synthesis of TMBs which otherwise takes days relying on high temperature conditions alone.[3] However, a disadvantage is using large, sophisticated machinery for such reactions which make it very expensive, albeit being able to synthesize materials in bulk.[3] Some other examples of synthesis approaches are ball milling to produce crystalline TMBs, chemical vapor deposition (CVD), solid state metathesis, Sn-flux synthesis, carbothermal reduction, and borothermal reduction,[3,14,19,20] which all employ high temperature and/or high pressure conditions to synthesize TMBs in bulk, as nanostructures or as thin films. A more facile synthetic approach involves electrodeposition, a method which can easily be done in room temperature and pressure conditions in a short amount of time, and allows for manipulation of elemental concentrations by changing electrolyte concentration as demonstrated by Ahn *et al.* with Co-B-P catalysts.[3,19,20] The disadvantages of this method are the precursors need to be very specific, it relies on electric power and cannot be used for large scale synthesis.[3,14,19,20] All these different approaches result in different morphology for TMBs which result in different functionality for said TMBs.

Another potentially facile way of synthesizing TMBs is through solution-phase chemical reduction – using strong borohydrides to reduce metal salts and thus obtaining pure metal borides.[3,19,20] The general reduction can be shown using the equation below:

$$4M^{2+} + BH_4^- + 8OH^- \longrightarrow 4M + BO_2^- + 6H_2O$$

In this method the borohydride is used in excess compared to the metal precursor, to act as an abundant boron source and so that no metal ions are left unreacted.[19] The reaction can in principle be done at room temperature however, in general, it is exothermic and rapid, forming black solution and precipitates.[19] The big disadvantage is that the products are amorphous and need annealing, or other processing to produce crystalline phases.[19,20]

Brown *et al.* investigated this method on different nickel (II) salts – nitrates, acetates, chlorides, and sulfates to investigate the activity of catalytic hydrogenation and they were successful in reducing all the salts with sodium borohydride solution.[22] Similarly Los and Lasia *et al.* were successful in synthesizing amorphous Ni_2B reducing nickel acetate with sodium borohydride solution, which showed higher HER activity than Ni powder.[19] Li *et al.* were also successful in synthesizing FeB_2 using $LiBH_4$, however as mentioned all these TMBs needed to be annealed at high temperatures (300 ºC or higher) for further experimentation on HER, OER, hydrogen storage, etc.[3,19,20]

To circumvent this need for post-synthetic annealing, Schaak *et al.* proposed a direct solution synthesis approach to make nanocrystal structures of Ni_3B.[23] This approach was inspired by Schaak *et al.* own earlier research on synthesizing phase pure nanocrystalline intermetallic powders such as M-Sn (M = Ag, Au, Co, Cu, Fe, Ni), Pt-M' (M' = Bi, Pb, Sb, Sn) and Co-Sb bimetallic systems.[24] The modified polyol approach allows for controlling the size and shape of the nanoparticles – one that can be applied to TMB synthesis for their various applications as well.[24] In the direct solution method, the reaction follows the steps of nucleation into aggregation and then a smoothing to form Ni-B alloy nanoparticles that come

together to form a larger metal boron network, thus avoiding the need for any annealing afterward.[23] Schaak proposed the following three-step mechanism to form the metal borides shown in scheme 1below[23]:

$$BH_4^- + 2H_2O \xrightarrow[280^oC]{TEG,\ N_2} BO_2^- + 4H_2 \quad (1)$$

$$BH_4^- + 2Ni^{2+} + 2H_2O \xrightarrow[280^oC]{TEG,\ N_2} 2Ni + BO_2^- + 4H^+ + 2H_2 \quad (2)$$

$$BH_4^- + H_2O \xrightarrow[280^oC]{TEG,\ N_2} B + OH^- + 2.5H_2 \quad (3)$$

Scheme 1: Hypothesized three step reaction mechanism that lead to reduction of metal ion from chloride precursor and incorporation of boron from borohydride to form metal boride.[23]

Steps 2 and 3 are the most important in the direct solution method as it shows the reduction of metal ions and the incorporation of boron.[23] This method is done at fairly low temperatures, and the success of nickel it can indicate towards similar success with other transition metals such as cobalt, iron, zirconium etc.[23,24]

The research described in this thesis was inspired by Schaak's seminal method of direct solution synthesis of Ni_3B. I examined the direct solution synthesis of nickel, cobalt, zirconium, and nickel-zirconium bimetallic borides. I explored both Schlenk line synthesis in high boiling point solvents and a modification using solvothermal reactors to create a high-temperature, high-pressure environment using a low boiling point solvent to facilitate the synthesis of boride materials. In the following sections, I describe the experimental methods and the results of the syntheses, including physical and electronic structure characterization using powder X-ray diffraction, electron microscopy, and X-ray photoelectron spectroscopy. With the research showing promising results, future directions for developing this synthesis for applications in hydrogen storage – one that has not been possible on metal borides besides MgB_2, and in electrocatalysis – perhaps bifunctionality in HER and OER are warranted.

Experimental Methods

General information:

All x-ray diffraction (XRD) was done using Bruker D8 Microfocus instrument with Dectris Pilatus 3R 100K-A 2D detector with a 0.154 nm wavelength. XRD measurements were taken from 16 – 93° theta range with increments of 5.5 degrees and 45 seconds for each step using 1mm collimator. XRD samples were prepped by placing sample powders onto silicon wafers. Cobalt boride was analyzed with 7500 eV threshold to suppress fluorescent signal from sample and remaining samples were analyze with 4800 eV threshold. XRD references were taken from DIFFRAC.EVA software PDF-4 2023 database with reference numbers for each compound below:

Table II. Table of compounds used as reference from DIFFRAC.EVA database with reference numbers

Name	Reference number in DIFFRAC.EVA
Ni metal	PDF 00-004-0850
Ni_3B	PDF - 04-014-0853
$Ni_3(BO3)_2$	PDF 00-022-0745
ZrB_2	PDF 00-034-0423
ZrO_2	PDF 00-036-0420
Co_2B	PDF 04-001-0966
KCl	PDF 00-004-0587

All XPS spectra samples were taken on a Kratos Axis-Ultra DLD spectrometer. This instrument has a monochromatized Al Kα X-ray and a low energy electron flood gun for charge neutralization. X-ray spot size for these acquisitions was on the order of 700 x 300 μm. The electrostatic lens was used for data collection. Pressure in the analytical chamber during spectral acquisition was less than 5 x 10-9 Torr. Pass

energy for survey spectra (composition) was 160 eV. Pass energy for the high-resolution spectra was 40 eV. For cobalt boride samples pass energy for survey and detailed spectra (composition) was 80 eV. Pass energy for the high-resolution spectra was 20 eV. The take-off angle (the angle between the sample normal and the input axis of the energy analyzer) was 0º (0-degree take-off angle ~ 100 Å sampling depth). The Kratos Vision2 software program was used to determine peak areas and to calculate the elemental compositions from peak areas. CasaXPS was used to peak fit the high-resolution spectra. For the high-resolution spectra, a Shirley background was used and all binding energies were referenced to the C ls C-C bonds at 285.0 eV.

XPS spectra were referenced from National Institute of Science and Technology (NIST) database (www.srdata.nist.gov/xps/selEnergyType.aspx) and Surface Science Western laboratories at University of Ontario (www.xpsfitting.com) database.

All reagents were purchased from Sigma Aldrich and used as is.

Experiment 1: Synthesis of nickel boride nanoparticles using direct solution synthesis method

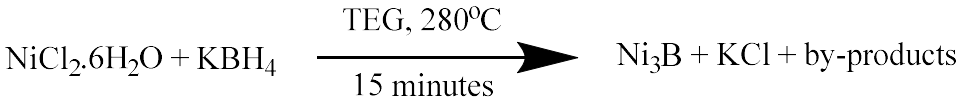

Scheme 2: Ni_3B direct solution synthesis scheme

KBH_4 (99.9% purity, 0.5035g or 9.5 mmol) was mixed in tetraethylene glycol (TEG) (99% purity, 15 mL), sonicated and left stirring overnight under nitrogen gas to dissolve fully. $NiCl_2.6H_2O$ (99.99% purity, 0.1195g or 0.50 mmol) was also mixed separately in the same volume of TEG in a 3-neck flask and left to stir overnight under nitrogen to dissolve fully. The following day the KBH_4 solution was chilled in an ice bath for 30 minutes, and the $NiCl_2$ solution was heated to 60ºC and let to cool down to 45-50ºC. Once the $NiCl_2$ solution temperature dropped, the chilled KBH_4 solution was added to the $NiCl_2$ solution, and the total mixture is then heated to 280ºC for 15 minutes, while keeping stirring under nitrogen. After heating

was completed, the solution was left to cool to room temperature, and the solution was separated into 4 centrifuge tubes for workup. Toluene was added to precipitate the products followed by centrifuging at 11,000 rpm for 20 minutes. Two rounds of toluene addition were needed to crash out the mixture. After decanting the toluene supernatant, the samples were each washed with ethanol and centrifuged under the same conditions. Approximately 8 washes of ethanol were needed to achieve a clear supernatant, indicating impurities, unreacted products and unwanted salts were completely washed away. A portion of final sample was reserved for XRD analysis.

Experiment 2: Synthesis of zirconium boride using direct solution synthesis method

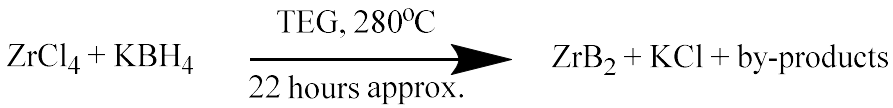

Scheme 3: ZrB_2 direct solution synthesis scheme

Anhydrous $ZrCl_4$ (99.9% purity, 0.1285g or 5.51 mmol) was mixed in TEG (99% purity, 15 mL), sonicated and left to stir overnight under nitrogen in a 3-neck flask to dissolve fully. KBH_4 (99.9% purity, 0.5008g or 9.28 mmol) solution was made in same volume of TEG, sonicated and left to stir under nitrogen overnight to dissolve fully as well. The following day, the $ZrCl_4$ solution was heated to 60°C and left to cool, while the KBH_4 was placed in an ice bath. With the $ZrCl_4$ solution cooling down to 45-50°C, the KBH_4 solution was transferred, and the total mixture was heated to 280°C, continuing the stirring and nitrogen flow. The mixture was left to heat overnight (approximately 22 hours total) and the following day the reaction was stopped and let to cool down to room temperature. The crude reaction was separated into 4 centrifuge tubes and washed with different solvents – ethanol, DI water, acetonitrile, and n-hexanes. DI water provided successful crash out, with which the reaction mixture was washed 4 times. XRD, SEM, TEM and XPS of the final cleaned product was obtained.

Experiment 3: Synthesis of cobalt boride using direct solution synthesis method

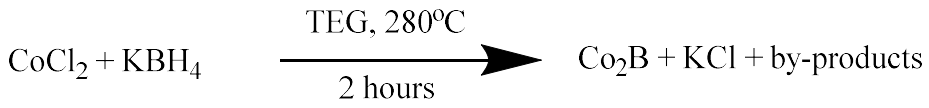

Scheme 4: Co_2B direct solution synthesis scheme

$CoCl_2$ (99.9% purity, 0.0626g or 4.82 mmol) was mixed in TEG (99% purity, 15 mL), sonicated and left to stir overnight under nitrogen in a 3-neck flask to dissolve fully. KBH_4 (99.9% purity, 0.5020g or 9.30 mmol) was also mixed in same volume of TEG, sonicated and left to stir under nitrogen overnight. The following day, the KBH_4 solution was placed in an ice bath and the $CoCl_2$ solution was heated to 60°C and left to cool down to 45-50°C, after which the KBH_4 solution was transferred onto the $CoCl_2$ solution. The total mixture was heated to 280°C, and it was heated for 2 hours total, continuing stirring and nitrogen flow. After 2 hours of heating the solution was left to cool down to room temperature. Final cooled solution was separated into 6 centrifuge tubes of 5 mL volume approximately each, and the workup with toluene and ethanol was done in the same process from experiment 1. 3 toluene washes were needed to crash out the solution and afterwards 8 ethanol washes were needed after which point the supernatant was clear. The final product was obtained for XRD, SEM, TEM and XPS analysis. A portion of the final product was also annealed at 600°C for 2 hours and an XRD was done of the annealed sample.

Experiment 4: Synthesis of nickel boride using direct solution synthesis method in solvothermal reactor

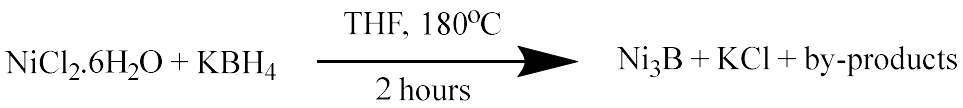

Scheme 5: Ni_3B direct solution synthesis scheme in solvothermal reactor

$NiCl_2.6H_2O$ (99.9% purity, 0.0587g or 2.47 mmol) was mixed in tetrahydrofuran (THF) (99% purity, 7.5 mL), sonicated and stirred overnight under nitrogen. KBH_4 (99.9% purity, 0.2515g or 4.66 mmol) solution was also made in the same manner with THF and left to stir overnight under nitrogen. The following day the KBH_4 solution was chilled in ice bath and added to the $NiCl_2$ solution. The total 15 mL mixture was transferred to a solvothermal reactor vessel, and the reactor was sealed and placed in oven. The reactor was heated to 180 ºC for 2 hours after which the heating was stopped, and the vessel was allowed to cool down to room temperature overnight. The following day the crude reaction solution was transferred to two centrifuge tubes and washed with toluene once. The supernatant was clear after one wash, and sample was analyzed with XRD, SEM, TEM and XPS.

Experiment 5: Synthesis of nickel-zirconium bimetal boride using direct solution synthesis method in solvothermal reactor

$$NiCl_2.6H_2O + ZrCl_4 + KBH_4 \xrightarrow[\text{2 hours and 22 hours approx.}]{\text{THF, } 180^oC} \text{Ni-Zr-B} + KCl + \text{by-products}$$

Scheme 6. Ni-Zr-B direct solution synthesis scheme using solvothermal reactor

Anhydrous $ZrCl_4$ (99.9% purity, 0.0887g or 3.81 mmol) and $NiCl_2.6H_2O$ (99.9% purity, 0.1296g or 5.45 mmol) were together mixed in THF (99% purity, 15mL), sonicated and left to stir overnight under nitrogen. KBH_4 (99.9% purity, 0.5287g or 9.80 mmol) was dissolved in same volume of THF, sonicated and stirred overnight as well. The following day, the KBH_4 was chilled in ice bath and then transferred to the mixed $ZrCl_4$ and $NiCl_2$ solution. The total mixture was then transferred to two different solvothermal reactor vessels, and the reactors were heated to 180ºC. Reactor 1 was heated for 2 hours and reactor 2 was left to heat overnight (approximately 16 hours). After heating both reactors were stopped and allowed to cool to room temperature, solutions from each reactor were transferred to two separate centrifuge tubes for each

and washed with toluene. Supernatant was clear after one wash and portion of two different final products were obtained for XRD, SEM, TEM and XPS analysis.

Results and Discussion

Experiment 1: Synthesis of nickel boride nanoparticles using direct solution synthesis method

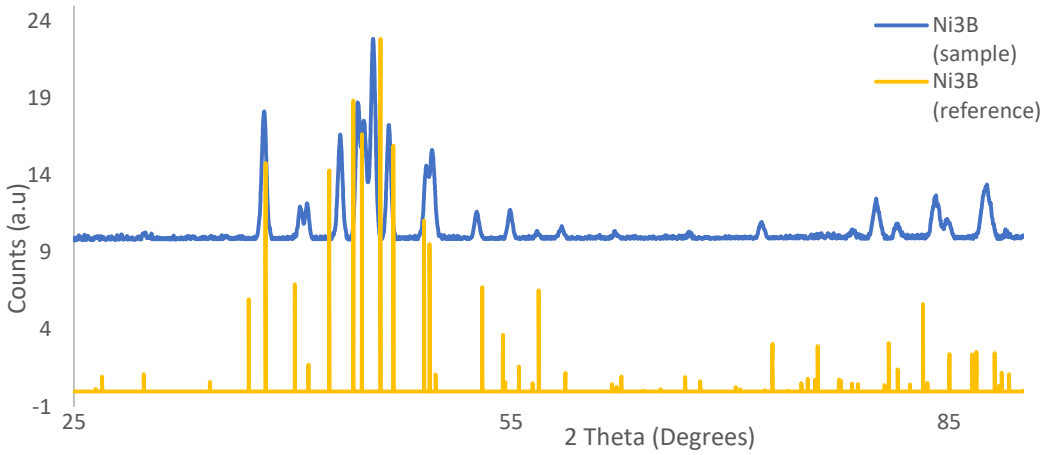

Figure 12. Sample Ni_3B XRD peak compared with reference Ni_3B XRD from database.

The observed XRD peaks in figure 12 of the sample at 38°, 40°, 41°, 44°, 45°, 47°, 50°, 52°, 55°, 70°, 80°, 85° and 87° are similar to the reference peaks of Ni_3B with some minor shifts, a result consistent with the original report from Schaak. The observed shifts can be fit to extract lattice parameters as shown in table III below:

Table III. Table of calculated sample lattice parameters with literature values of Ni_3B from Diffrac.EVA software database:

Parameters	calculated	literature
a (Å)	5.06209	5.2219
b (Å)	6.68085	6.6171
c (Å)	4.44721	4.3918

The shifts and minor changes in relative peak intensities can be potentially explained due to nanostructuring and nonstoichiometry. With the result being in line with the Schaak *et al.* experiments it was concluded the reaction method works and the research proceeded to synthesize the next target materials – zirconium boride and cobalt boride. The research on zirconium and cobalt was motivated by the fact they are earth abundant 3d orbital transition metals, and their amorphous metal borides have previously been successful in OER applications.[25]

Experiment 2: Synthesis of zirconium boride using direct solution method

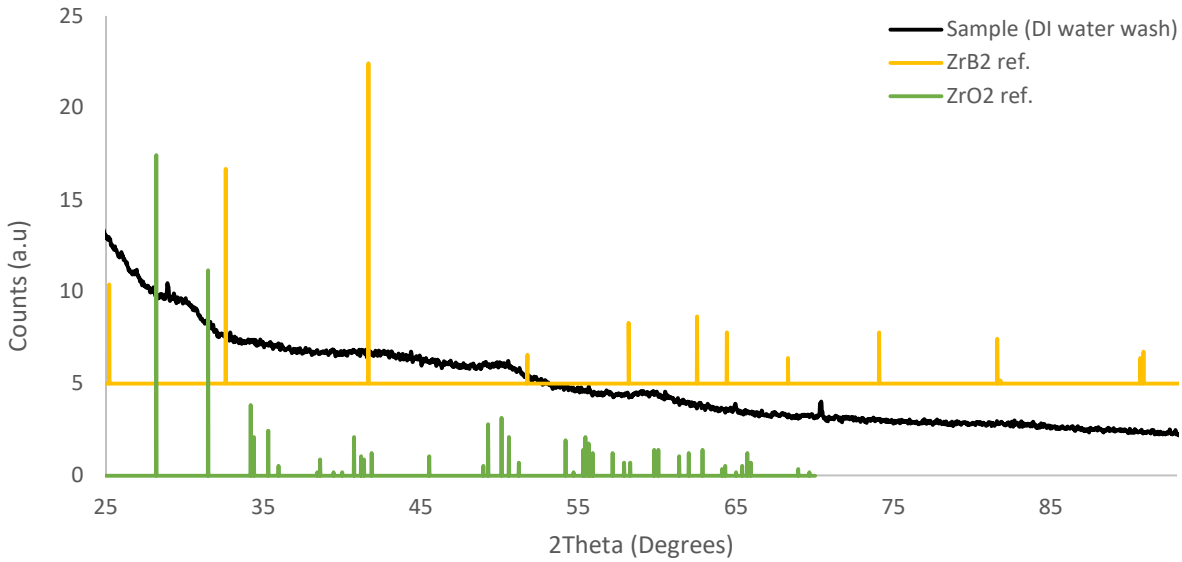

Figure 13. Sample ZrB_2 peak compared with database reference peaks

The XRD pattern in figure 13 showed either low intensity signals or broad signals, a phenomenon suggestive of an amorphous sample or the generation of small nanoparticles with broad signals that are not readily observed above background. The small nanoparticles were confirmed by TEM imaging in figure 14, and from a high magnification TEM image the average particle size was measured to be 3.3 nm and some faint lattice fringes observed where the gaps measured to be 0.28 nm:

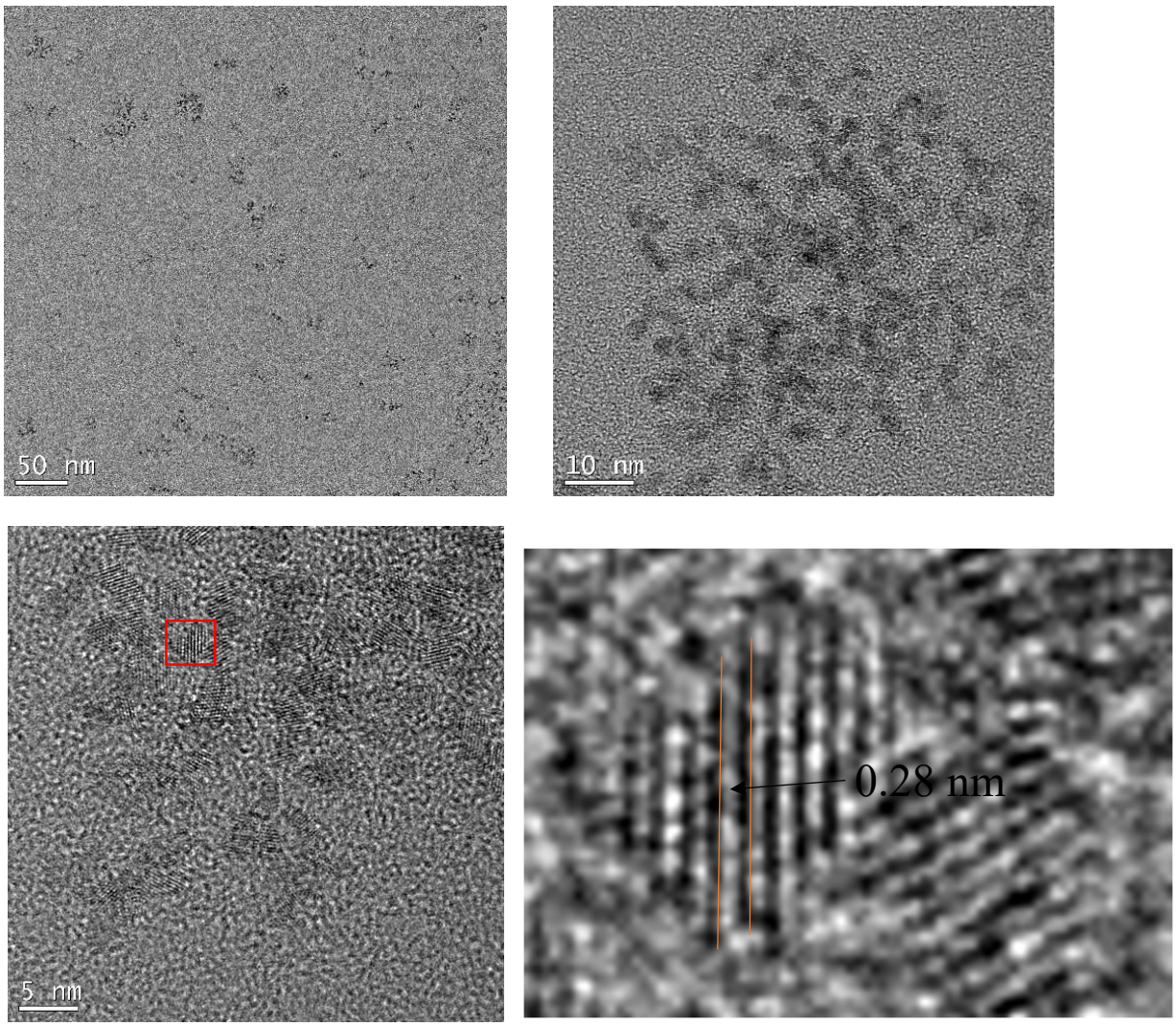

Figure 14. (Top left) 50 nm scale TEM image of sample particles. (Top right) 10 nm scale TEM image of sample particles. (Bottom left) 5 nm scale TEM images of sample particles with region used to measure lattice fringes marked in red square. (Bottom right) zoomed in section of 5 nm scale image from which lattice fringe gap measurement of 0.28nm was taken.

These lattice gaps are similar to previously reported value of 0.29 nm approximately by Sigwadi *et al.* on their synthesized ZrO_2 nanoparticles, which can indicate the material in the experiment synthesized is very small ZrO_2 particles.[26] When the ZrO_2 peaks from XRD database was referenced with the sample, it gave a slightly better understanding of the sample XRD pattern. The small broad peaks over 30°, 40°, 50° and 60° 2 theta region align with the ZrO_2 reference patterns as well as the very faint peaks at 55° and 65° 2 theta region. The small particle size can definitely be the reason why the spectrometer cannot detect distinct

singular peaks over said regions from the sample itself. EDS of TEM (region used for EDS shown in figure S3) confirmed the presence of both zirconium and boron with atom% values shown in table IV:

Table IV. EDS results from TEM showing atom% of Zr and B present in the sample.

Element	Atom%
B	37.27
Zr	59.25

However, XPS analysis (survey scan shown in figure S2) only showed signal from Zr as shown in the figure 15 below:

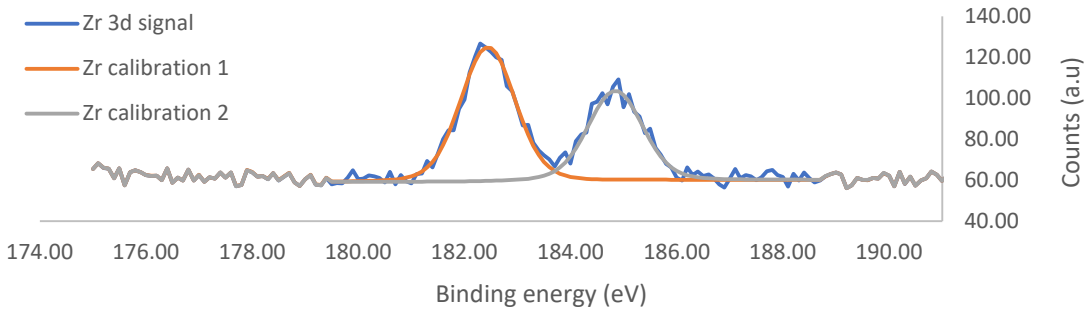

Figure 15. Hi-res scan of ZrB_2 3d orbital with peaks at 182.4 eV and 184.8 eV. No boron signal was detected in sample.

The observed zirconium signal, when compared with database peaks, showed the same asymmetric doublet shape, with the 3d 5/2 peak signal at 182.4 eV and the 3d 3/2 peak signal at 184.8 eV - both values close to ZrO_2 peak values of 182.3 eV and 185.5 eV, suggesting an oxidation state of +4 for Zr. The zirconium peak values being close to ZrO_2 also reinforce the result of ZrO_2 formation rather than ZrB_2. The boron signal not being detected can be because XPS is a particle surface based analytical technique and with our materials being very small and scattered throughout, it is difficult for the spectrometer detect. Formation of zirconium oxide could also be a reason as the oxide layer on the surface, can prevent any boron signal to

be detected by the spectrometer. An SEM was done of the sample as well to understand its morphology with a representative image shown below in figure 16:

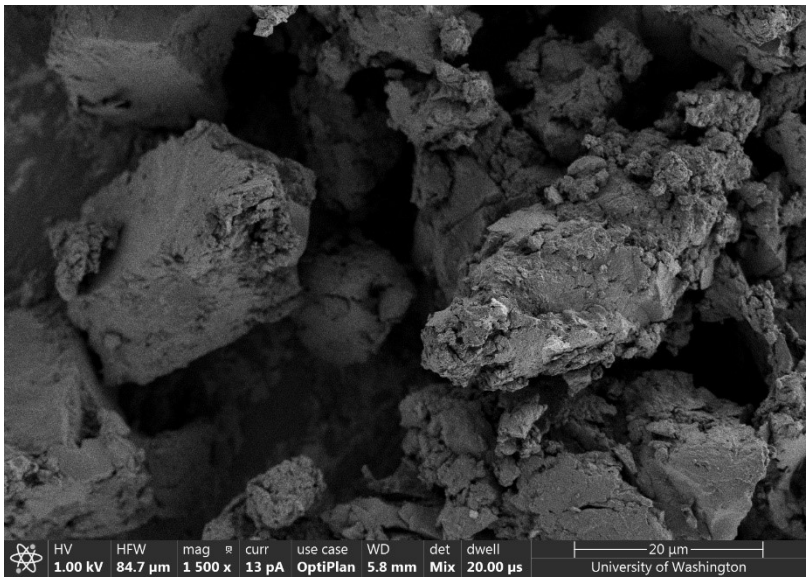

Figure 16. SEM image of sample ZrB_2 particles at 6500x magnification. Sample was crushed onto aluminum stub for preparation and SEM imaging was taken.

The sample at high magnification appears to be consistent with a powdery solid. The EDS (shown in figure S1) showed zirconium at 6.2 wt% in the sample. However, boron's signal in general is at quite low energy (0.18 keV) and can be challenging to detect via SEM due to overlap with carbon. TEM and XPS are better analytical techniques to detect boron presence in compounds.

The experimental results point towards formation of ZrO_2 instead of expected ZrB_2. This outcome can have occurred from the water, produced by TEG breaking down at high temperatures over long period of time, reacting with reduced zirconium metal. $ZrCl_4$ the precursor, is also very water soluble and potentially some of the unreacted reagents ended up reacting with water in the solvent creating the oxide product instead. A repeat of the experiment with a solvent that won't introduce water is necessary for a better synthesis approach. With this result, we turned to the synthesis of cobalt boride.

Experiment 3: Synthesis of cobalt (II) boride using direct solution synthesis method

The initially obtained product showed a general lack of clear XRD signals, similar to previous experiment. Annealing was a step necessary in normal chemical reduction synthesis of metal borides to obtain the crystalline materials from amorphous compounds[22]. To try and crystallize the material, the sample was annealed at 600 °C for 2 hours under argon, and the sample XRD was taken again, giving the pattern in figure 17 below:

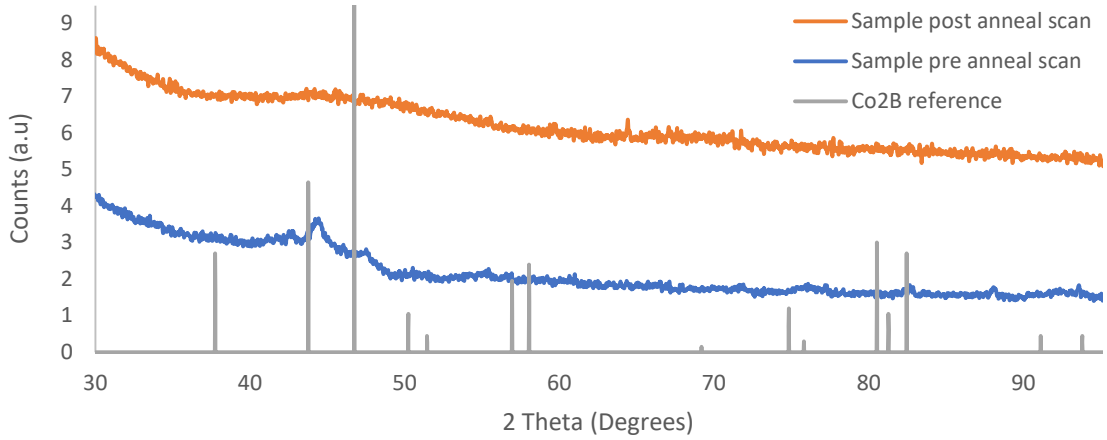

Figure 17. Co_2B sample XRD graph before and after annealing product compared with database Co_2B XRD pattern.

In both cases the sample remained amorphous to analyze by XRD. After annealing the two low peaks between 42°- 47° had disappeared and became a broad peak over the region. Annealing may have resulted in formation of small crystalline particles similar to experiment 2 that would not be identifiable by XRD. As such SEM and XPS analysis were done on pre-annealed sample and neither method picked up a signal for cobalt or boron in sample (figure S4 and S5). The SEM EDS detected presence of other metals, which could be contaminants from SEM detector itself. High magnification SEM image showed powdery solids similar to the experiment 2 sample in figure 18:

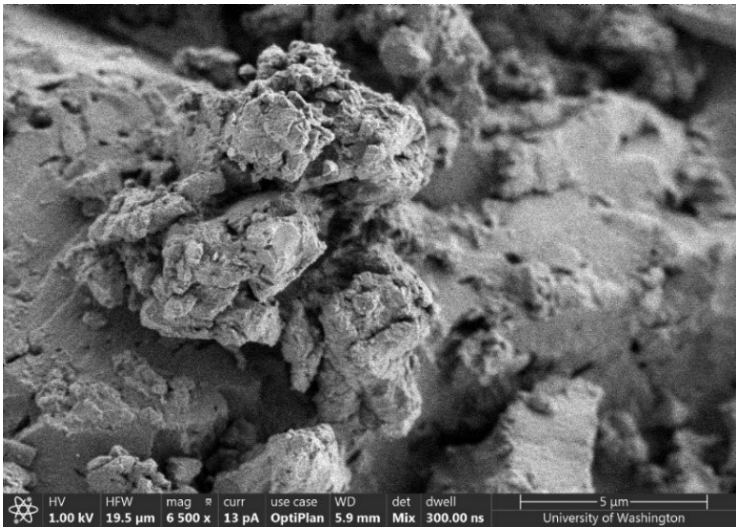

Figure 18. SEM image of sample Co_2B at 6500x magnification. Sample was crushed onto aluminum stub for preparation and SEM imaging was taken.

Unlike the previous two experiments, the cobalt experiment did not appear successful in giving a crystalline boride phase by direct solution synthesis. It is unclear as to why this result occurred – besides synthesizing very small particles unable to be properly detected by XRD, the SEM EDS and XPS analysis not detecting any cobalt or boron presence needs to be investigated. Perhaps there was an experimental setup error where there was air exposure that resulted in oxidation of materials, or $CoCl_2$ in presence of TEG has an unexpected reaction. An analysis such as NMR, could be done on the $CoCl_2$ precursor to ensure there was no contaminants present there as well. SEM and XPS of the post annealed product and comparing with the pre annealed product could provide better understanding of what the outcome of the experiment is. Keeping those factors in mind the research was moved onto the next method – to carry out direct solution synthesis in solvothermal reactors. Solvothermal reactors would allow for us to do multiple reactions with varying conditions or reagents simultaneously and potentially at lower temperature than a Schlenk line setup. The reactor being a closed system would create a HPHT environment which in general helps in synthesis of metal borides. The reaction medium would also be changed to use tetrahydrofuran (THF) instead of TEG – this would prevent introduction of excess water in the sample to create unwanted side reactions.

Experiment 4: Synthesis of nickel boride using direct solution synthesis method in solvothermal reactor

The first synthesis done in this manner was re-doing the Ni_3B as it provides a good baseline for comparison. The XRD of the initial product obtained after one crash out is shown below in blue and is compared with the nickel boride synthesized with the normal reaction method in experiment 1 in orange in figure 19:

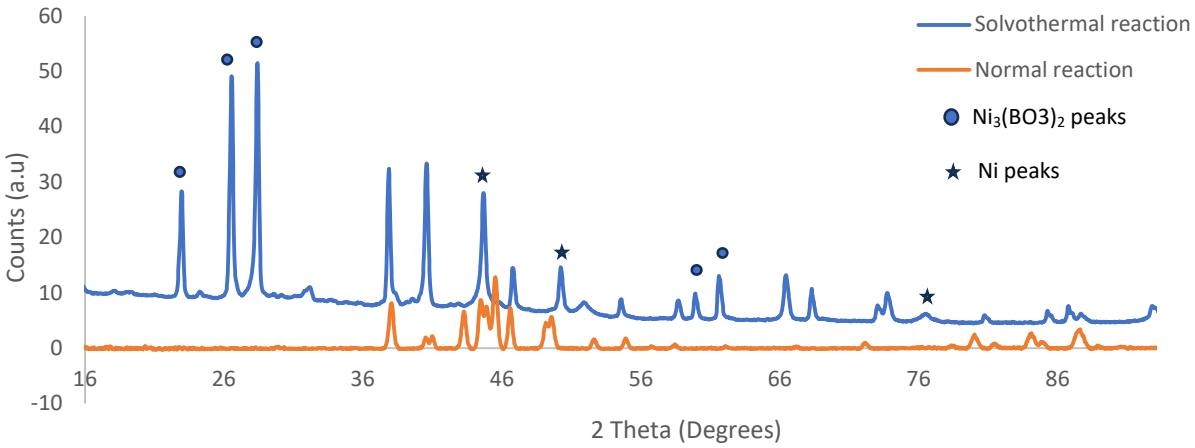

Figure 19. XRD scan of sample Ni_3B synthesized using solvothermal reactor and compared with XRD of Ni_3B prepared in experiment 1. Peaks marked with circle were hypothesized to be of nickel borate and peaks marked with star were hypothesized to be of nickel metal.

While some of the Ni_3B peaks were observed in the sample there were new peaks observed as well. Unlike the Ni_3B sample from experiment 1, the current sample only had 5 singlet peaks between 37° – 50° and in the lower 2 theta region three singlet peaks at 20° - 30° and 4 singlet peaks from 60° – 70° which were not present for experiment 1 sample. Comparing to literature nickel borate and nickel peaks reported by Wang *et al.* in synthesis of nickel borate nanowhiskers,[27] the three single peaks at 45°, 76° and 51° corresponded to nickel metal peaks confirmed by referencing from databases as well in figure 20. The sample XRD pattern mostly matched with nickel borate pattern as well - the two single peaks from 20° – 26°, single peak at 40°, two peaks at 60° and 61° and the two peaks at 72° and 73° corresponded to nickel borate however,

the two nickel borate signal that are supposed to be present at 33° is absent in the sample and instead a singular broad signal at 32° is observed in figure 20

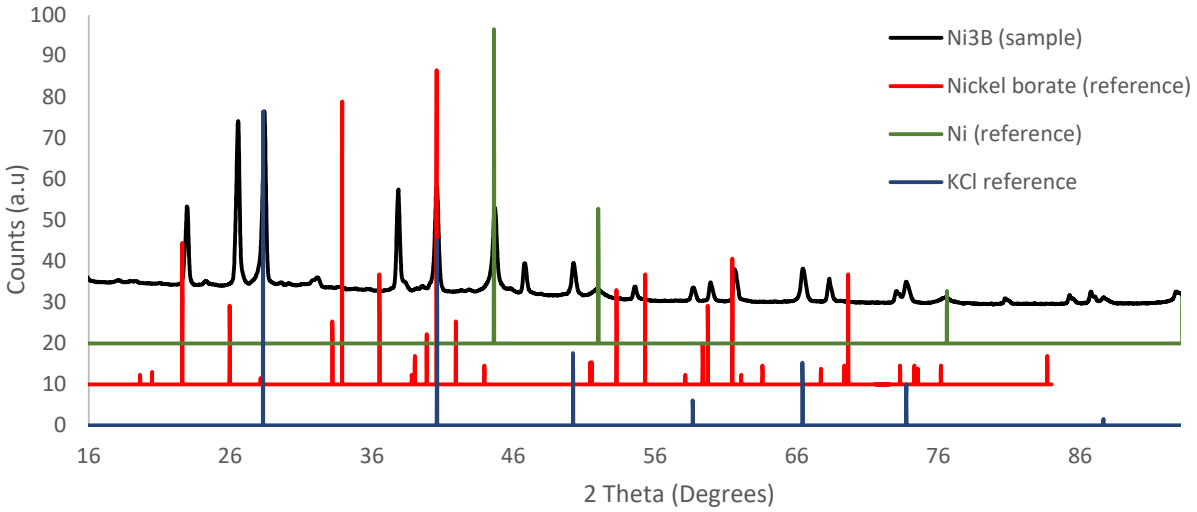

Figure 20. Sample XRD peaks compared with nickel borate and nickel metal database peaks.

The sample pattern peak still had peaks present that are still not identifiable by referencing with known nickel boride or borate variants. SEM of the sample was done with the particles appearing thin plate like structures shown in figure 22 and the EDS also confirmed presence of nickel however, it also showed high presence of potassium chloride in the sample (figure S6) – 32.5 wt% K and 31.9 wt% Cl. When the XRD pattern was referenced with potassium chloride, the remaining unaccounted for peaks at 28°, 40°, 50°, 58°, 66°, and 73° aligned perfectly, as seen in figure 20.

This meant that the sample was still impure with by-products, mainly with potassium chloride. The toluene wash while precipitated the materials, it did not wash away the salt and further washes with polar organic solvent will be needed in future experiments. The XRD pattern from figure 20 also confirms presence of some nickel borate and it is unclear why the formation occurred in the first place. One possibility is the presence of water from the nickel chloride hexahydrate reagent. Research previously done by Klabunde *et al.* have previously shown that borates are intermediates to borides when prepared in water.[28] The presence

of borate could indicate the reaction also did not reach completion with 2 hours of heating. In fact, the absence of the two 33° 2 theta peaks in sample could allude to the sample being reaction intermediate and some nickel borate was reacting towards a complete product – which resulted in a shift to a singular broad signal at 32°. Still to get a better understanding of the structure and morphology of the formed material TEM and XPS was done as well.

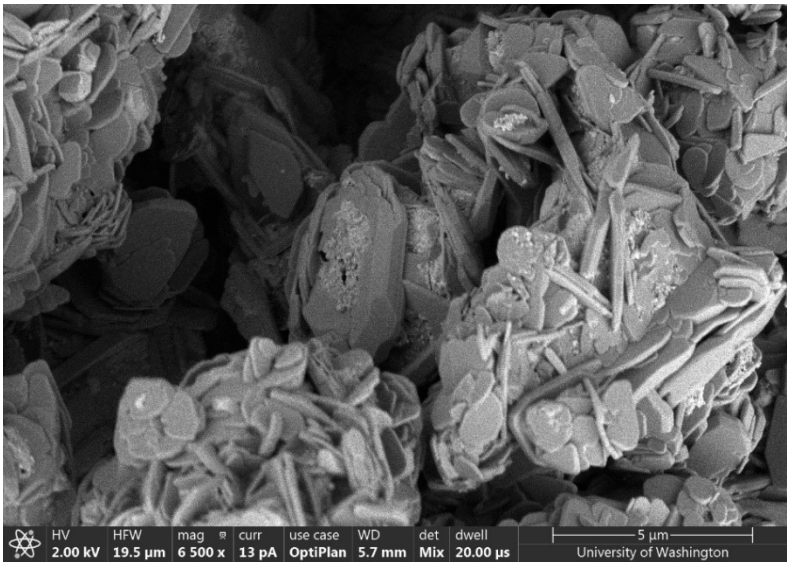

Figure 21. SEM image of experiment 4 sample at 6500x magnification. Sample was crushed onto aluminum stub for preparation and SEM imaging was taken. Particle shape appears to be thin plate like structures.

TEM imaging of the sample showed polydispersed large particles in figure 22:

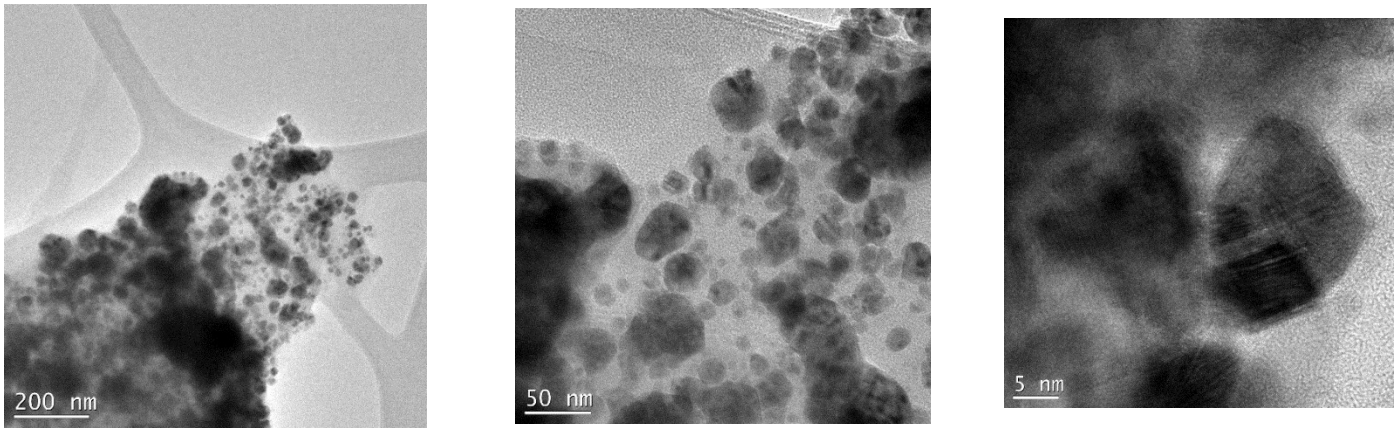

Figure 22. TEM images of experiment 4 sample at (left) 200 nm scale, (middle) 50 nm scale and (right) 5 nm scale. Particles appear to be polydispersed throughout and some lattice fringes can be observed although not fully clear.

The particles at low magnification (200 nm scale) are much larger than experiment 2 sample particles. Overall, the images show presence of organic materials due to the general lack of clarity of the particles themselves. Some faint lattice fringes can be observed in the high magnification (5 nm scale) image; however, they are not clear to analyze using imaging software. EDS from the TEM (figure S8) revealed very high atom % of nickel present shown in table V:

Table V. EDS results from TEM showing atomic% of Ni and B present in sample.

Element	Atom%
B	2.47
Ni	95.30

From the XRD data this also further reinforces the hypothesis that the reaction did not reach completion even with 2 hours of heating. The high presence of nickel can be explained the overall chemical reduction process only completed the metal reduction step and the reaction was incomplete. While both nickel and boron were detected via compositional analysis, XPS analysis also confirmed the presence of borate seen in figure 23, after the oxidation state was cross referenced from databases (figure S7):

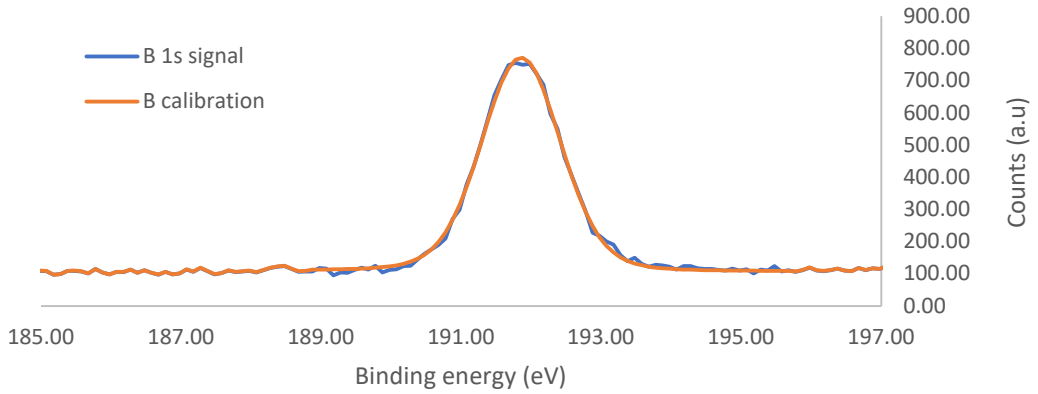

Figure 23. Hi-res scan showing boron 1s orbital signal after calibration having binding energy of 191.98 eV

Boron's 1s signal at 191.98 eV is shifted from the 187 eV for borides – towards a value that corresponds more with B_2O_3 when referenced with databases. Signal for nickel from the 855 – 880 eV region was too noisy to analyze significant peaks to understand the oxidation state as seen in figure 24:

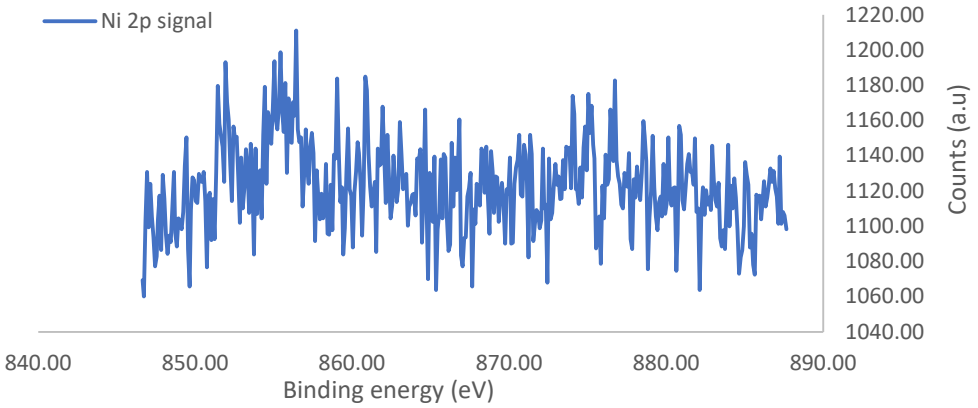

Figure 24. Hi-res scan showing nickel 2p orbital signal. Ni signal too noisy to analyze

Nickel signal being noisy could be attributed to the sample impurity as well. Nickel borate, nickel metal, potassium chloride mask away the nickel signal – the overall survey scan (figure s7) does show high intensity peaks of by-products and salts. Overall, it can be concluded that the experiment was incomplete and the sample analyzed was mixture of intermediate products. It will be important to explore the dependence of this reaction on time and other synthesis parameters to see if pure phase nickel boride is accessible. At this point, however, the research proceeded to the final experiment – bimetallic metal boride synthesis using nickel and zirconium. The bimetal boride synthesis would allow for exploration into longer period of heating and a medium that won't introduce water to react with zirconium precursor.

Experiment 5: Synthesis of nickel-zirconium bimetal boride using direct solution synthesis method in solvothermal reactor

Sample XRD from reactor 1 (2-hour experiment) was the nearly the same as experiment 4 Ni_3B sample as seen from figure 25 below:

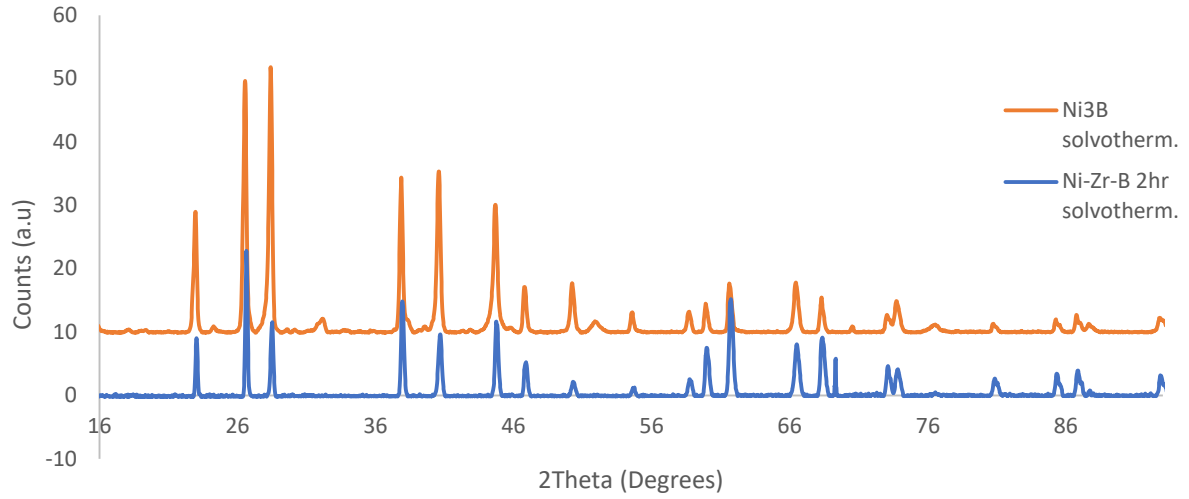

Figure 25. Bimetallic boride sample heated for 2 hours XRD compared with solvothermal Ni_3B XRD peaks. Peak pattern appears identical with difference in intensity of peaks.

It was hypothesized that the mixture of zirconium and nickel together would result in doping and that may be the case given the subtle differences in peak intensities and positions observed. To test whether further conversion could be achieved, we examined the same reaction overnight and the overnight sample XRD was different compared to 2 hour heated sample XRD in figure 26:

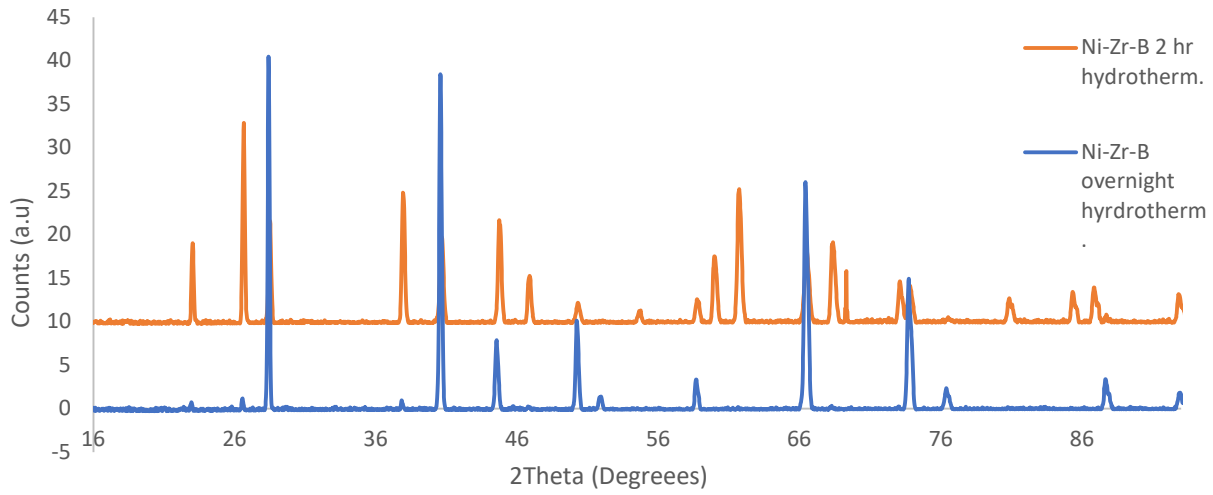

Figure 26. Two different bimetallic boride syntheses XRD pattern compared. Majority of nickel borate peaks appear gone after 22 hours of heating.

The lower 2 theta peaks that are attributed to nickel borate were gone and several peaks between 46° and 61° were also gone. When comparing the overnight sample XRD pattern to database patterns, the sample pattern was corresponded to the Ni and KCl patterns shown in figure 27:

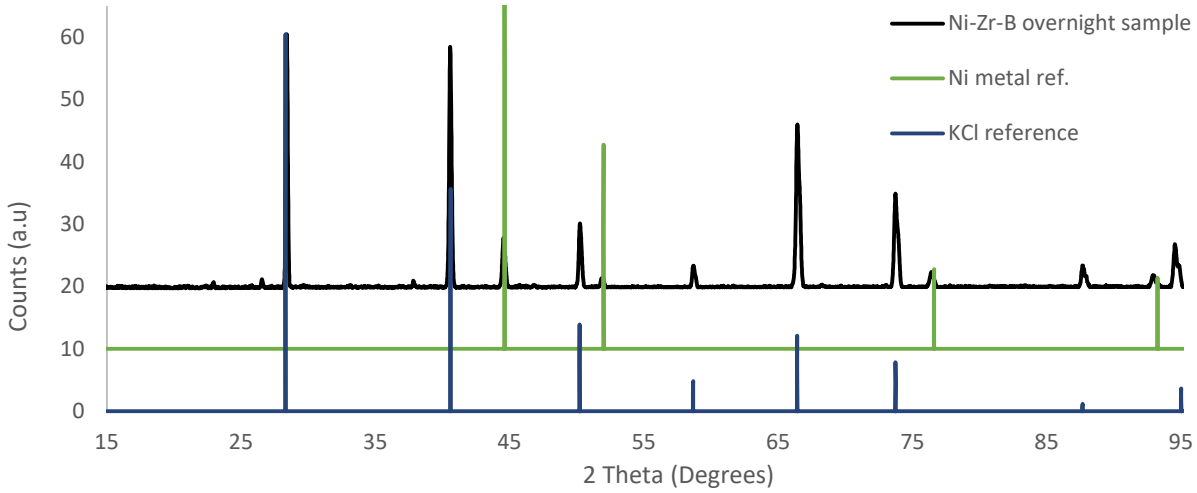

Figure 27. Overnight heating sample XRD compared with metallic nickel and KCl database peaks.

There is evidence of metallic nickel with peaks at 44°, 52°, 77° and 93° and the remaining peaks at 28°, 40°, 50°, 58°, 66°, 73°, 87° and 94° all correspond to KCl. The sample showing KCl is again attributed to toluene

not being a solvent appropriate for washing the sample but rather just precipitating it, and washes with ethanol is needed in the future. However, the sample not showing the nickel borate peaks anymore suggest they have been converted likely into amorphous Ni_3B that cannot be identified by XRD. This would also be consistent with previous research by Klabunde *et al.*[28] The high presence of KCl and metallic nickel can also be masking the synthesized nickel boride signals, which have some peaks that overlap with the other species. The total ratio of metal precursor (nickel and zirconium chloride) to borohydride in the experiment amounted to 1:1, which would not be sufficient for metal boride synthesis. Borohydride needs to be in excess because it serves as a reducing agent and boron source – as a result the end product of this reaction shows high presence of metallic nickel. Other analyses were still done to understand the morphology and structure of synthesized particles. SEM image obtained is shown in figure 28 below:

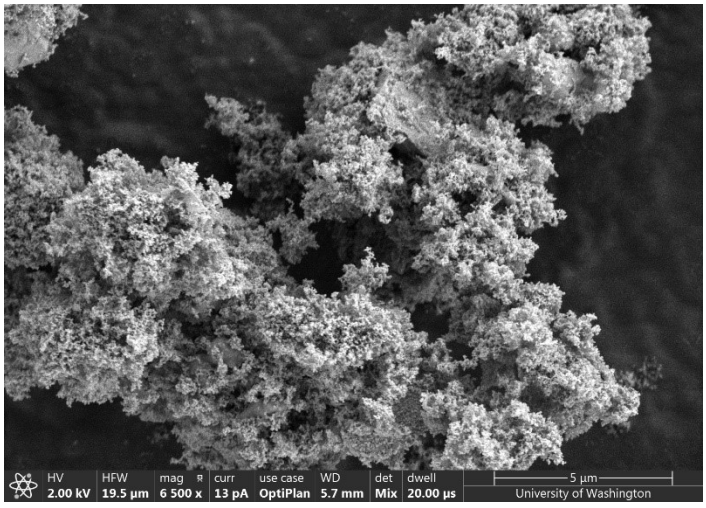

Figure 28. SEM image of Ni-Zr-B sample heated overnight at 6500x magnification. Sample was prepared by crushing onto stub.

The particles appear as mesh like solids unlike the long, thin plate like structures in experiment 4 sample and EDS confirmed Zr and Ni (figure S9) signals which was also confirmed by XPS analysis compositional analysis as well. SEM EDS and XPS (figures S9 and S10) also confirmed the presence of boron and KCl impurities as well.

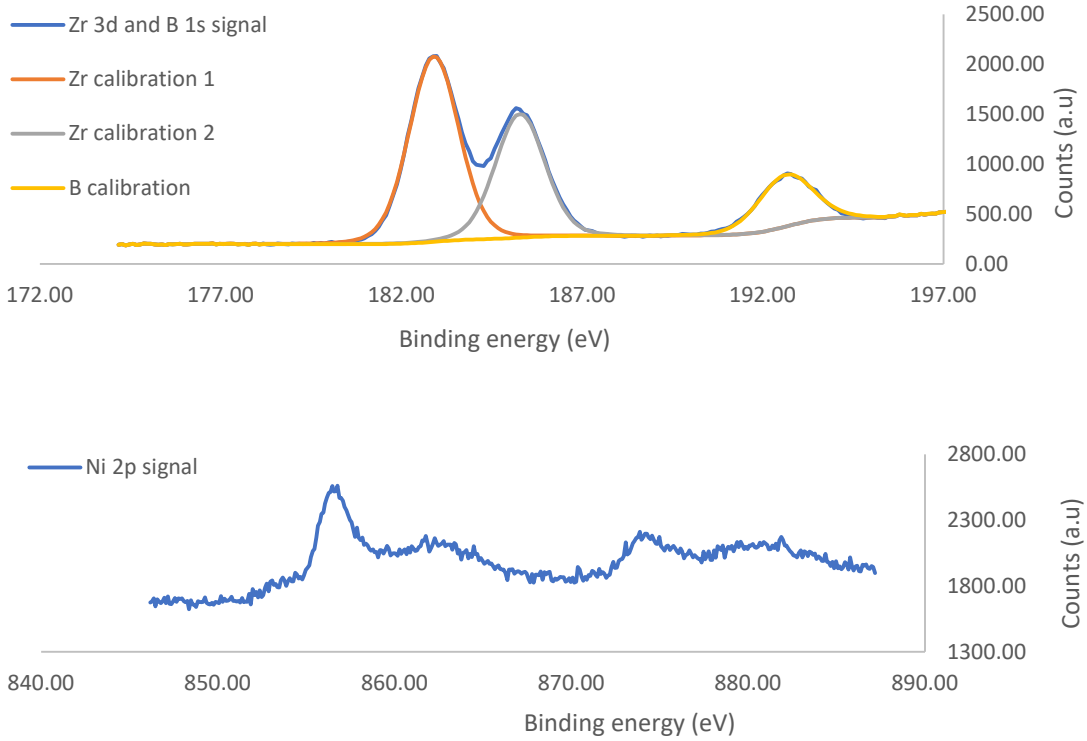

Figure 29. (Top) Hi-res scans showing zirconium 3d signals at 182.5 eV and 185 eV and boron 1s signal at 192 eV. (Bottom) Hi-res scan showing nickel 2p signals peaks at 856 eV, 862 eV, 874 eV and 882 eV.

The boron and zirconium signal peaks in figure 29 are consistent with previous experimental XPS data – boron peak at 192 eV indicating B_2O_3 which would explain the lower region 2 theta XRD peaks. The 3d 5/2 Zr signals after calibrating were at 182.5 eV a value close to $ZrCl_4$ binding energy of 183.7 eV– suggesting an oxidation state of +4 for zirconium in the sample. The binding energy value similarity could mean the zirconium did not end up reacting from reagents as well, due reaction not having sufficient borohydride present. However, there is no XRD pattern to help with the conclusion, as the sample peak pattern are those of Ni and KCl. The nickel XPS signal is clearer now compared to experiment 4 and when comparing to database values, one peak signal at 856 eV, the broad peak over 862 eV, and other peaks at

874 eV, 882 eV values that are similar to $Ni(OH)_2$ - indicating an oxidation state of +2 for nickel. The reaction overall cannot be concluded to have worked in creating doped products or individual metal borides however, the longer heating did generate a product with a greater consumption of the nickel borate, which merits further investigation. Properly washing the materials with ethanol to remove the KCl will also make sample better to interpret by TEM, SEM, XPS and XRD. Annealing at high temperatures may also be required if the sample product still appears to be amorphous after purification to obtain crystalline products.

Conclusions

Direct solution synthesis is a facile and potentially versatile method to make transition metal borides. My results have shown that Schlenk line synthesis at 280 °C produces nanocrystals of Ni_3B, consistent with previous studies, as well as ~3 nm particles of ZrO_2. The modification of using solvothermal reactors to do the synthesis at lower temperature using high pressure conditions is a potential avenue for further development. My results show evidence of borate and boride phases, but further exploration of reaction time and temperature is needed. Brown *et al.*'s previous success in chemically reducing other nickel salts e.g., nitrates and sulfates, is good motivation for exploring different salt precursors in both the Schlenk line and HPHT reactor setups. THF as reaction medium provided for easiest precipitation of products from the crude mixture however, washes with polar organic solvent such as ethanol is still necessary to wash away impurities and by-products, mostly of which is KCl as observed from EDS and XRD data. The cobalt boride synthesis was not successful in generating crystalline products, however that reaction is worth re attempting using the solvothermal reactor method and if successful another bimetallic boride synthesis can also be explored using nickel and cobalt. As mentioned before regarding bimetallic boride syntheses, the borohydride and metal precursor amount needs to be adjusted so that the borohydride is in excess as it serves two purposes – to reduce the metal ion and provide the boron source. Solvothermal reactions yielded best results with longer periods of heating. This method shows promise for creating boride and borate nanomaterials directly in the solution phase. We are excited about the prospects of developing this work further in the coming years to generate new nanoscale materials for hydrogen storage and production.

References

(1) Murthy, T. S. R. C.; Sonber, J. K.; Sairam, K.; Majumdar, S.; Kain, V. Boron-Based Ceramics and Composites for Nuclear and Space Applications: Synthesis and Consolidation. In *Handbook of Advanced Ceramics and Composites*; Mahajan, Y. R., Johnson, R., Eds.; Springer International Publishing: Cham, 2020; pp 703–738. https://doi.org/10.1007/978-3-030-16347-1_22.

(2) Scheifers, J. P.; Zhang, Y.; Fokwa, B. P. T. Boron: Enabling Exciting Metal-Rich Structures and Magnetic Properties. *Acc. Chem. Res.* **2017**, *50* (9), 2317–2325. https://doi.org/10.1021/acs.accounts.7b00268.

(3) Ma, T.; Zhu, P.; Yu, X. Progress in Functional Studies of Transition Metal Borides*. *Chin. Phys. B* **2021**, *30* (10), 108103. https://doi.org/10.1088/1674-1056/ac1925.

(4) Greenwood, N. N.; Parish, R. V.; Thornton, P. Metal Borides. *Q. Rev. Chem. Soc.* **1966**, *20* (3), 441. https://doi.org/10.1039/qr9662000441.

(5) Lee, E.; Fokwa, B. P. T. Nonprecious Metal Borides: Emerging Electrocatalysts for Hydrogen Production. *Acc. Chem. Res.* **2022**, *55* (1), 56–64. https://doi.org/10.1021/acs.accounts.1c00543.

(6) Wang, Q.; He, J.; Hu, W.; Zhao, Z.; Zhang, C.; Luo, K.; Lü, Y.; Hao, C.; Lü, W.; Liu, Z.; Yu, D.; Tian, Y.; Xu, B. Is Orthorhombic Iron Tetraboride Superhard? *J. Materiomics* **2015**, *1* (1), 45–51. https://doi.org/10.1016/j.jmat.2015.03.004.

(7) Burdett, J. K.; Canadell, Enric.; Miller, G. J. Electronic Structure of Transition-Metal Borides with the AlB2 Structure. *J. Am. Chem. Soc.* **1986**, *108* (21), 6561–6568. https://doi.org/10.1021/ja00281a020.

(8) Frotscher, M.; Hölzel, M.; Albert, B. Crystal Structures of the Metal Diborides ReB2, RuB2, and OsB2 from Neutron Powder Diffraction. *Z. Für Anorg. Allg. Chem.* **2010**, *636* (9–10), 1783–1786. https://doi.org/10.1002/zaac.201000101.

(9) Wang, S.; Yu, X.; Zhang, J.; Zhang, Y.; Wang, L.; Leinenweber, K.; Xu, H.; Popov, D.; Park, C.; Yang, W.; He, D.; Zhao, Y. Crystal Structures, Elastic Properties, and Hardness of High-Pressure Synthesized CrB2 and CrB4. *J. Superhard Mater.* **2014**, *36* (4), 279–287. https://doi.org/10.3103/S1063457614040066.

(10) *Structural variations, relationships and properties of M2B metal borides | Elsevier Enhanced Reader*. https://doi.org/10.1016/j.jssc.2018.12.014.

(11) Carenco, S.; Portehault, D.; Boissière, C.; Mézailles, N.; Sanchez, C. Nanoscaled Metal Borides and Phosphides: Recent Developments and Perspectives. *Chem. Rev.* **2013**, *113* (10), 7981–8065. https://doi.org/10.1021/cr400020d.

(12) Akopov, G.; Yeung, M. T.; Sobell, Z. C.; Turner, C. L.; Lin, C.-W.; Kaner, R. B. Superhard Mixed Transition Metal Dodecaborides. *Chem. Mater.* **2016**, *28* (18), 6605–6612. https://doi.org/10.1021/acs.chemmater.6b02632.

(13) Wort, C. J. H. Applications for Superhard and Ultra-Hard Materials. In *Microstructure-Property Correlations for Hard, Superhard, and Ultrahard Materials*; Kanyanta, V., Ed.; Springer International Publishing: Cham, 2016; pp 25–74. https://doi.org/10.1007/978-3-319-29291-5_2.

(14) Pu, Z.; Liu, T.; Zhang, G.; Liu, X.; Gauthier, Marc. A.; Chen, Z.; Sun, S. Nanostructured Metal Borides for Energy-Related Electrocatalysis: Recent Progress, Challenges, and Perspectives. *Small Methods* **2021**, *5* (10), 2100699. https://doi.org/10.1002/smtd.202100699.

(15) Zhang, C.; He, X.; Liu, C.; Li, Z.; Lu, K.; Zhang, S.; Feng, S.; Wang, X.; Peng, Y.; Long, Y.; Yu, R.; Wang, L.; Prakapenka, V.; Chariton, S.; Li, Q.; Liu, H.; Chen, C.; Jin, C. Record High Tc Element Superconductivity Achieved in Titanium. *Nat. Commun.* **2022**, *13* (1), 5411. https://doi.org/10.1038/s41467-022-33077-3.

(16) Gok and Cihan / The International Journal of Materials and Engineering Technology 003 (2020) 109-119. **2020**.

(17) Guo, Z.; Zhou, J.; Sun, Z. New Two-Dimensional Transition Metal Borides for Li Ion Batteries and Electrocatalysis. *J. Mater. Chem. A* **2017**, *5* (45), 23530–23535. https://doi.org/10.1039/C7TA08665B.

(18) Gunda, H.; Ray, K. G.; Klebanoff, L. E.; Dun, C.; Marple, M. A. T.; Li, S.; Sharma, P.; Friddle, R. W.; Sugar, J. D.; Snider, J. L.; Horton, R. D.; Davis, B. C.; Chames, J. M.; Liu, Y.-S.; Guo, J.; Mason, H. E.; Urban, J. J.; Wood, B. C.; Allendorf, M. D.; Jasuja, K.; Stavila, V. Hydrogen Storage in Partially Exfoliated Magnesium Diboride Multilayers. *Small* **2023**, *19* (6), 2205487. https://doi.org/10.1002/smll.202205487.
(19) Gupta, S.; Patel, M. K.; Miotello, A.; Patel, N. Metal Boride-Based Catalysts for Electrochemical Water-Splitting: A Review. *Adv. Funct. Mater.* **2020**, *30* (1), 1906481. https://doi.org/10.1002/adfm.201906481.
(20) Jiang, Y.; Lu, Y. Designing Transition-Metal-Boride-Based Electrocatalysts for Applications in Electrochemical Water Splitting. *Nanoscale* **2020**, *12* (17), 9327–9351. https://doi.org/10.1039/D0NR01279C.
(21) Akopov, G.; Pangilinan, L. E.; Mohammadi, R.; Kaner, R. B. Perspective: Superhard Metal Borides: A Look Forward. *APL Mater.* **2018**, *6* (7), 070901. https://doi.org/10.1063/1.5040763.
(22) Brown, C. A. Catalytic Hydrogenation. V. Reaction of Sodium Borohydride with Aqueous Nickel Salts. P-1 Nickel Boride, a Convenient, Highly Active Nickel Hydrogenation Catalyst. *J. Org. Chem.* **1970**, *35* (6), 1900–1904. https://doi.org/10.1021/jo00831a039.
(23) Schaefer, Z. L.; Ke, X.; Schiffer, P.; Schaak, R. E. Direct Solution Synthesis, Reaction Pathway Studies, and Structural Characterization of Crystalline Ni $_3$ B Nanoparticles. *J. Phys. Chem. C* **2008**, *112* (50), 19846–19851. https://doi.org/10.1021/jp8082503.
(24) Cable, R. E.; Schaak, R. E. Low-Temperature Solution Synthesis of Nanocrystalline Binary Intermetallic Compounds Using the Polyol Process. *Chem. Mater.* **2005**, *17* (26), 6835–6841. https://doi.org/10.1021/cm0520113.
(25) Yang, Y.; Zhuang, L.; Rufford, T. E.; Wang, S.; Zhu, Z. Efficient Water Oxidation with Amorphous Transition Metal Boride Catalysts Synthesized by Chemical Reduction of Metal Nitrate Salts at Room Temperature. *RSC Adv.* **2017**, *7* (52), 32923–32930. https://doi.org/10.1039/C7RA02558K.
(26) Sigwadi, R.; Mokrani, T.; Dhlamini, M. The Synthesis, Characterization and Electrochemical Study of Zirconia Oxide Nanoparticles for Fuel Cell Application. *Phys. B Condens. Matter* **2020**, *581*, 411842. https://doi.org/10.1016/j.physb.2019.411842.
(27) Cao, J.; Wang, Y.; Song, X.; Feng, J. One-Dimensional Nickel Borate Nanowhiskers: Characterization, Properties, and a Novel Application in Materials Bonding. *RSC Adv.* **2014**, *4* (37), 19221–19225. https://doi.org/10.1039/C4RA01630K.
(28) Glavee, G. N.; Klabunde, K. J.; Sorensen, C. M.; Hadjipanayis, G. C. Borohydride Reduction of Cobalt Ions in Water. Chemistry Leading to Nanoscale Metal, Boride, or Borate Particles. *Langmuir* **1993**, *9* (1), 162–169. https://doi.org/10.1021/la00025a034.

Supplemental information:

Experiment 2: Synthesis of zirconium boride using direct solution synthesis method

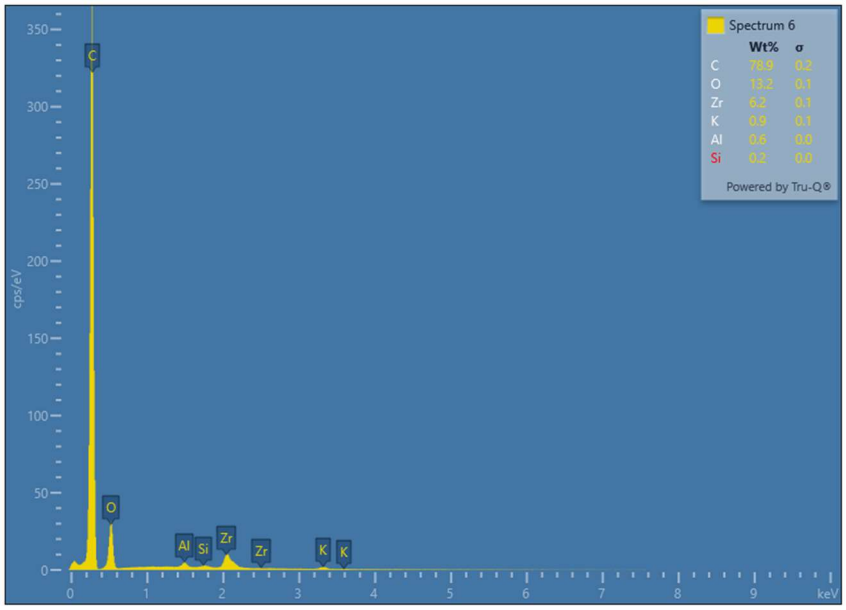

Figure S1. EDS data from SEM of ZrB_2 sample.

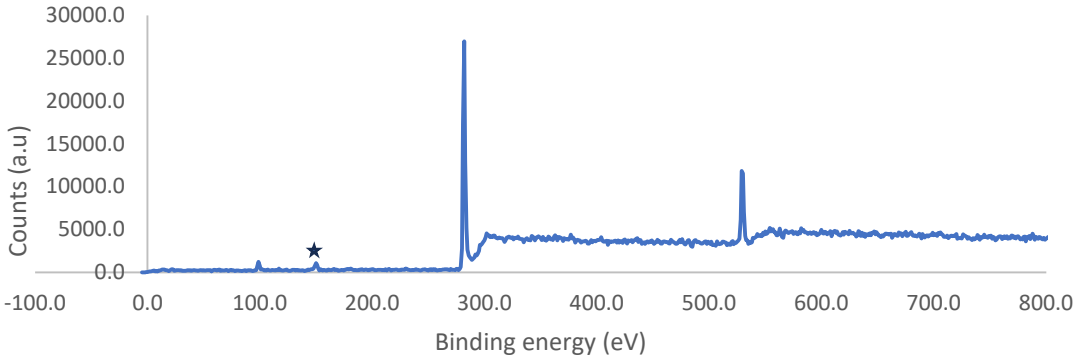

Figure S2. XPS survey scan of ZrB_2 sample. Peak for zirconium boride marked with star and peak for atmospheric carbon at 285 eV used to calibrate graphs marked with circle.

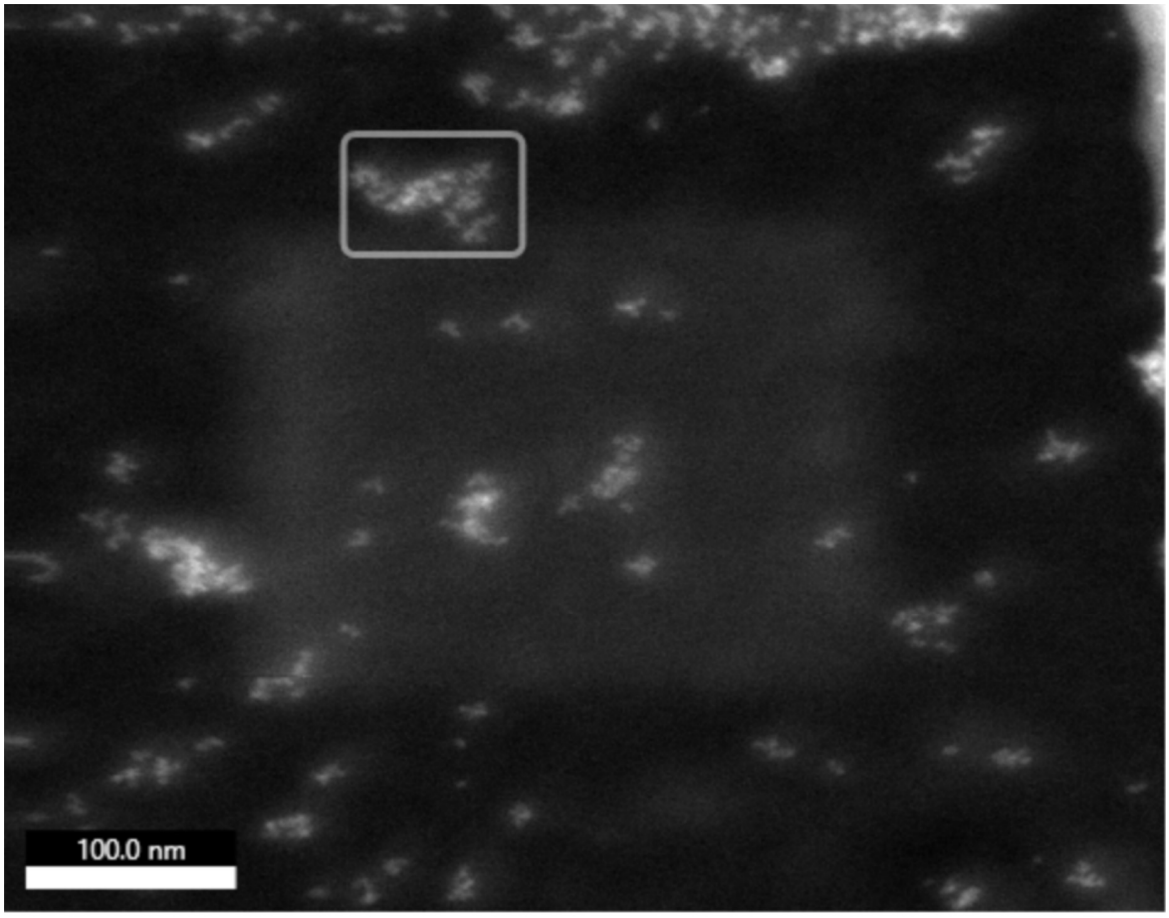

Figure S3. TEM image marking region where EDS for ZrB_2 sample was done.

Experiment 3: Synthesis of cobalt (II) boride using direct solution synthesis method

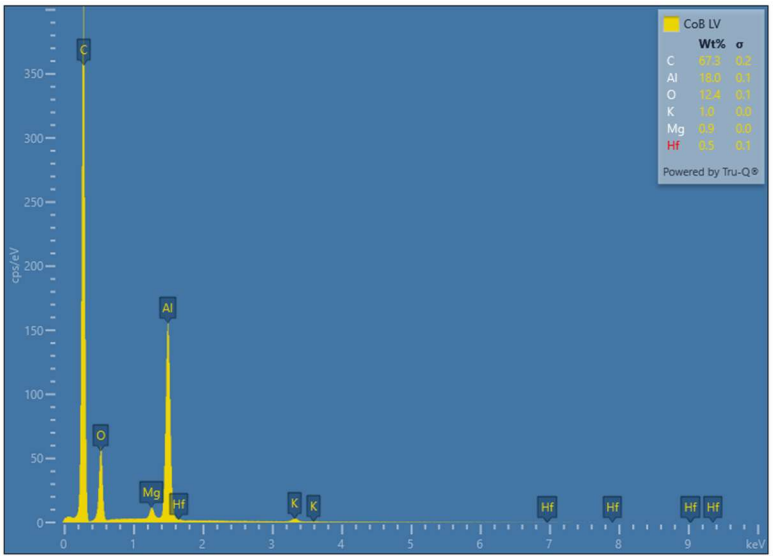

Figure S4. SEM EDS of Co_2B sample. No Co peaks detected.

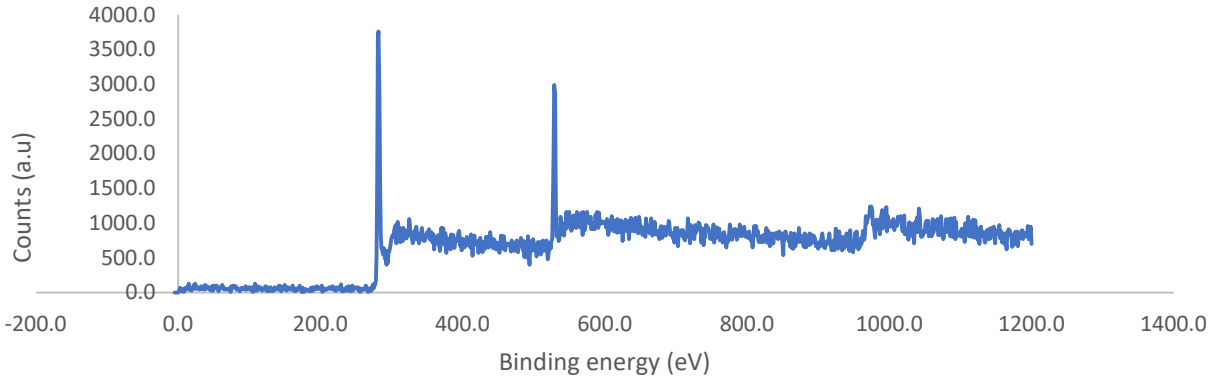

Figure S5. Survey scan for Co_2B sample. Standard atmospheric carbon peak at 285 eV observed and unknown 530 eV signal detected. No elemental peak from sample for cobalt or boron was detected.

Experiment 4: Synthesis of nickel boride using direct solution synthesis method in solvothermal reactor

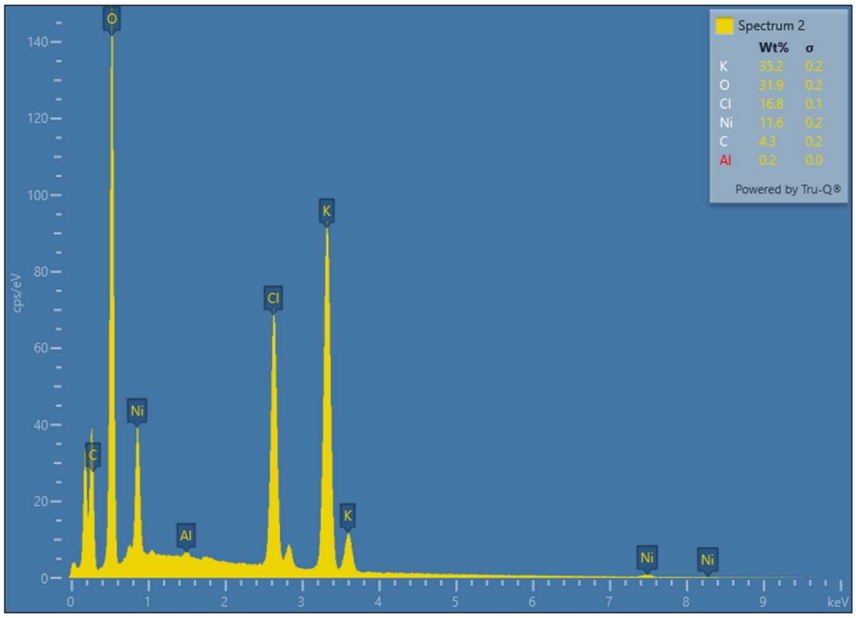

Figure S6. SEM EDS data of sample. Nickel was detected however high wt% of K and Cl detected indicating sample impurity.

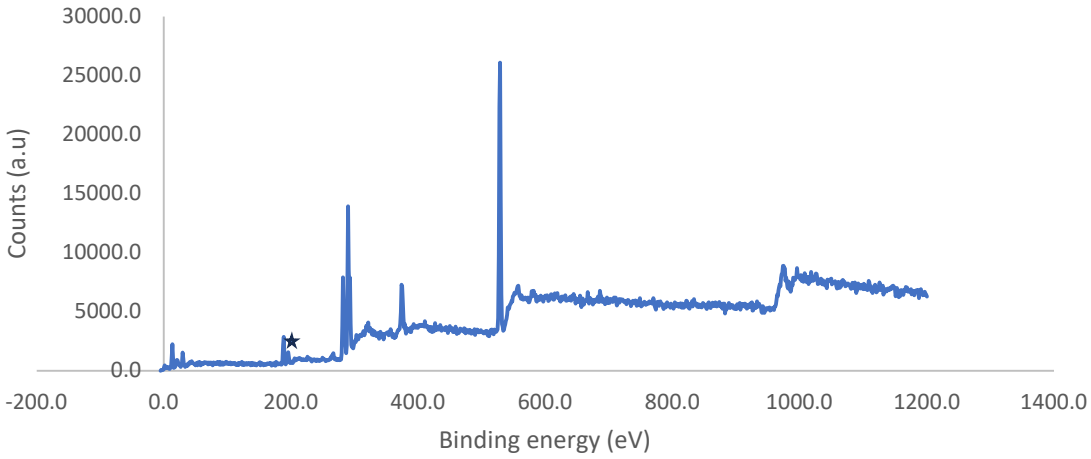

Figure S7. Survey scan for experiment 4 sample. Boron peak marked with star. Besides standard carbon peak at 285 eV other large peaks of impurities present throughout the sample.

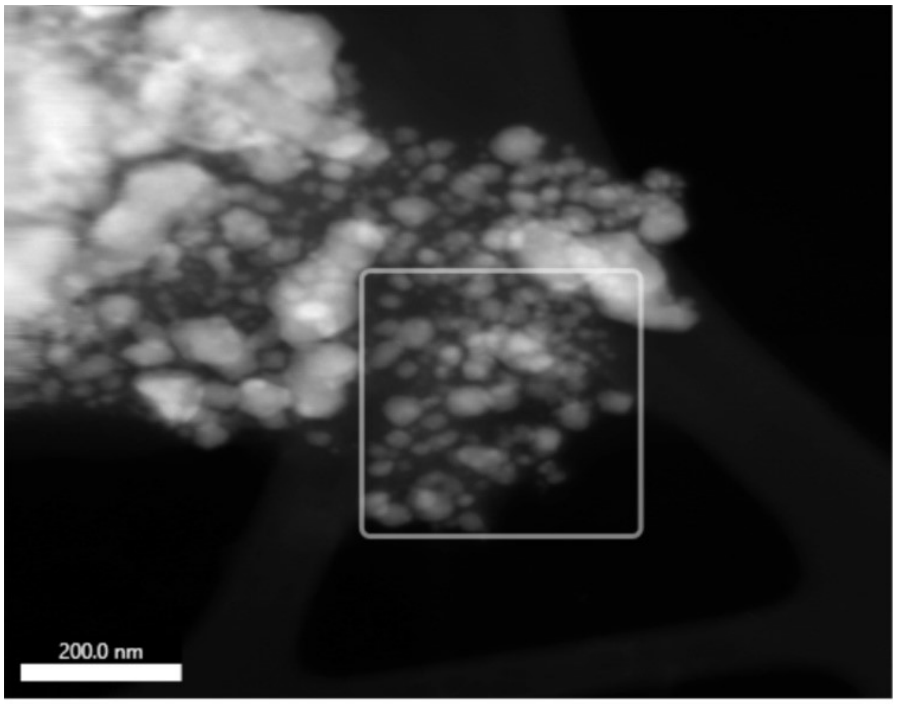

Figure S8. TEM image marking region where EDS was done for Ni_3B sample.

Experiment 5: Synthesis of nickel-zirconium bimetal boride using direct solution synthesis method in solvothermal reactor

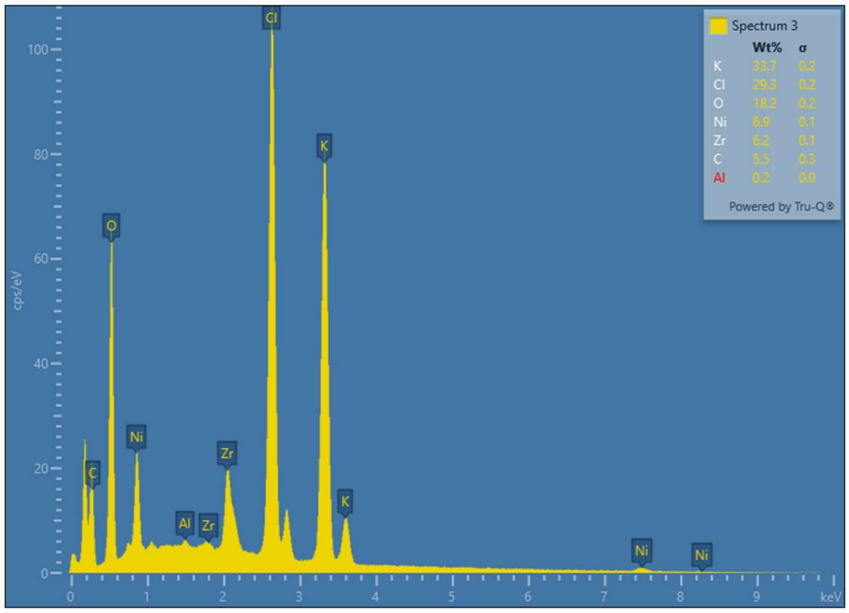

Figure S9. SEM EDS data indicating presence of both nickel and zirconium. Large peaks of potassium and chlorine also detected indicating sample heavily impure still.

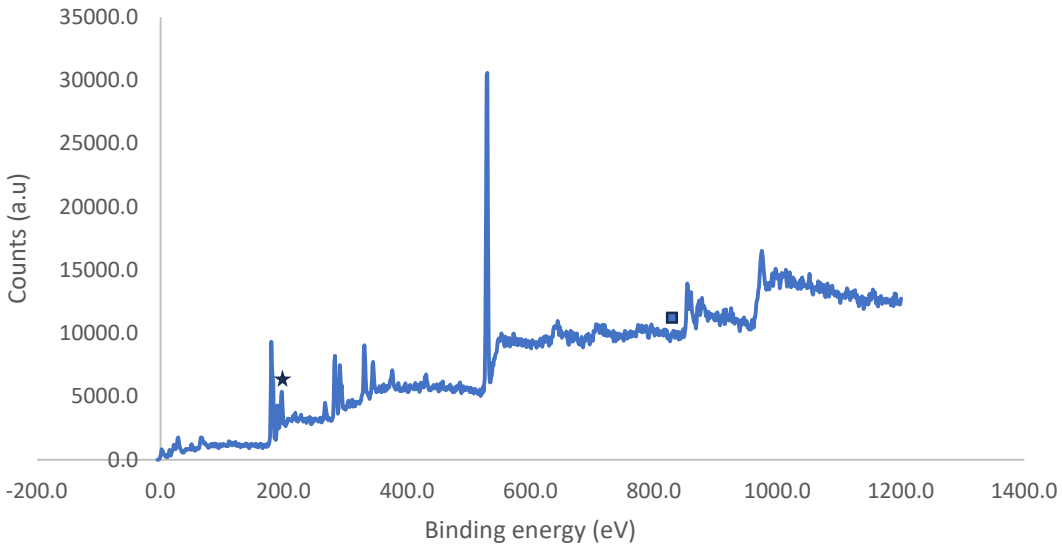

Figure S10. Survey scan for overnight heating of Ni-Zr-B sample. Zr and B signal region marked with star and Ni signal region marked with square. Standard carbon peak observed at 285 eV. Other by-product sample peaks present as well indicating sample impurity.